UNDERSTANDING THE ROLE OF SLAG ON GEOPOLYMER HARDENING AND MICROSTRUCTURAL DEVELOPMENT

BY

SRAVANTHI PULIGILLA

THESIS

Submitted in partial fulfillment of the requirements
for the degree of Master of Science in Civil Engineering
in the Graduate College of the
University of Illinois at Urbana-Champaign, 2011

Urbana, Illinois

Adviser:

Paramita Mondal

Abstract

The main objective of the present work was to understand the evolution of early age properties for successful application of geopolymer as an alternative binder. The early age properties like hardening (stiffening) and setting will determine the removal of formwork and thus the time of construction. The study was performed on user-friendly geopolymers obtained by using Class F flyash/slag/K-silicate/H_2O. This involves the use of low concentration alkaline activators and low-temperature curing. A detailed investigation of microstructural development and hardening rate was presented for flyash and slag based geopolymers. Flyash and slag precursors were treated with potassium hydroxide-silicate activator of modulus 1.25 keeping SiO_2/Al_2O_3 = 5.1. For the first time in this study, ultrasonic wave reflection method along with Proctor penetration were used to determine the stiffening rate of geopolymers and their results correlated well. Microstructural development was investigated using SEM/EDS while the reaction rate was monitored through the use of semi-adiabatic calorimetry. An increase in the stiffening rate was observed with the addition of slag. It was concluded that the calcium dissolving from slag influences the early age properties significantly. Possible hypothesis to explain the role of slag on microstructure development and increased rate of stiffening is presented. Microstructural changes responsible for hardening were studied by characterizing geopolymer solids using Fourier transform infrared spectroscopy (FT-IR). The main drawback of using FT-IR was that Si-O-T (T =Al, Si) vibrations from the initial ash, geopolymer product and calcium silicate hydrate, yields an overlapping spectrum bands resulting in a broad hump which is difficult to interpret. This was resolved by separating the spectrum by selectively dissolving calcium silicate hydrate and geopolymer product. Calcium silicate hydrate and geopolymer product were selectively dissolved by salicylic acid extraction method and hydrochloric acid respectively. These extraction methods revealed the presence

of calcium silicate hydrate in the samples supporting the theory. The pore solution extracted from geopolymer at various time intervals was also characterized through inductively coupled plasma spectroscopy for various ions like silicon, aluminum and calcium. As variation in ion concentrations was too high between multiple trials, no correlation could be established between the rate of product formation and change in ion concentration. The work on pore solution analysis will be repeated in the future after validating the test set up with more traditional system like cement paste and comparing data with existing literature.

Keywords: User friendly geopolymer, Ultrasonic Wave Reflection (UWR), flyash-slag geopolymer, hardening rate, salicylic acid methanol extraction method, Fourier transform infrared spectroscopy, pore solution extraction.

Acknowledgments

I would like to thank my supervisor, Prof. Paramita Mondal for her valuable guidance through the project. The independence she gave me right from choosing the topic to coming up with hypothesis has given me great confidence to grow as a researcher while enjoying all rigors of graduate student life. My transition from a bachelor student to a serious master's student could not have been smoother if not for her support and encouragement. I thank her for the financial support through the project.

I would also like to thank Prof. Leslie J. Struble. I have really enjoyed the two courses, characterization of construction materials and advanced cement chemistry which were taught by her. These two courses along with discussions with her have completely changed the way I think about research. I thank her for her valuable suggestions through the course of my project. I would like to thank Prof. Popovics and Prof. Struble for helping me with using Ultrasonic wave reflection method which has a special place in my research. I thank Prof. Paramita Mondal and Prof. John S. Popovics for letting me be a teaching assistant for CEE 300.

I would like to thank Prof. Timothy Strathmann and Dereck Vardon for letting me use their lab's FT-IR machine. I would like to thank Dr. Julio Soares, Dr. James Mabon and Dr. Mauro Sardela with their help on FT-IR, SEM and XRD machines in Fredrick Seitz Materials Lab. I would like to thank staff of Civil Engineering Department for being helpful in administrative matters.

Two years of my stay in UIUC has been amazing, I thank many of my friends who accompanied me through this journey. Some of my semesters have been very tough trying to manage as a teaching assistant, budding researcher and a student. I could have not been so successful without blessings of my parents and sister, my friends at UIUC and my closest buddies from my undergraduate.

Firstly, I wish to thank my parents and sister who are responsible for everything what I am today. I am really grateful for their support and being there at every moment of my life. I would like to specially thank Sriram, Pavani, Sailu, Neeha and Milli for their patience to listen through my ranting's on my toughest days and to share laughs on lighter days.

I would like to specifically thank my colleague Prannoy Suraneni, for his help with UWR, proctor, many hours of discussion on research and for his support and encouragement. This thesis would not have been completed without him.

I thank my group members Seungmin Lim, Pete Stynoski, Piyush Chaunsali and Bin Zhang for their suggestions during group meetings and for their friendship. I wish to thank my colleagues in the Civil Engineering Department for their friendship and the discussions for most of the courses we took together. Special thanks to my colleagues of CEE 300 who made TA job a lot of fun.

I wish to thank my friends at UIUC without whom my stay in USA would have been tough. I thank Rimpa, Sneha, Preeti, Sridhar, Rannesh, Adi, Ashna, Laavi, Som and Varun.

Table of Contents

List of Tables

List of Figures

Chapter 1

Research Motivation and Objective

When a highly concentrated aqueous alkali hydroxide-silicate solution is added to aluminosilicate raw material (metakaolin, flyash, slag), it results in an amorphous, three dimensional short range order inorganic polymer called 'geopolymer', after Davidovits[3]. There has been extensive research on the geopolymers made from metakoalin since their properties can be controlled for a given composition.[4] In contrast, geopolymers produced from flyash have variable properties depending on very broad particle size distribution of flyash particles and variable phase composition in different size fractions. For wide spread utilization of flyash, great amounts of research is needed.
The geopolymerisation process involves the use of chemical ingredients that may be dangerous and therefore require some safety procedures. The most commonly used soluble silicates with molar ratio (SiO_2:M_2O)< 1.45 are considered corrosive and must be handled with gloves, glasses and masks[3]. These requirements may inhibit the use of geopolymers in mass applications without proper safety procedures because they are not user-friendly. To utilize the full potential of geopolymer cements and to compete with Portland cement in terms of wide range of applications, geopolymers cements should be more user-friendly. Davidovits has emphasized the need for user friendly geopolymer by the use of discarded flyash as a aluminosilicate raw material thereby reducing the use of energy intensive and processed raw materials like metakaolin[3]. The user-friendly geopolymers are obtained by using Class F flyash/slag/K-silicate/H_2O and involves use of low concentration alkaline activators and low-temperature curing[5]. This is considered not just environment friendly but also user-friendly. Class F flyash is preferred over class C in user-friendly geopolymers because class C flyash requires high alkalinity to prevent any flash set during mixing[3]. Since class F flyash has very low amount of CaO, slag was added as the source of calcium ions and the properties can be controlled by varying the amount of slag added to the system.

The studies on metakoalin and slag systems have indicated that the calcium ions have a significant role in determining the properties at early ages as well as later ages. It is important to understand the role of calcium in optimizing the properties of user-friendly geopolmer systems. The main objective of the present research is to study the early age properties of flyash-slag geopolymer and explore the microstructural and chemical changes responsible for the hardening.

In order to achieve the objectives of this research, various experiments have been conducted. The current study involves the use of slag with various percentage replacements of flyash. Chapter 2 discusses existing literature on geopolymers, importance of user-friendly geopolymers, ultrasonic wave reflection method and some preliminary tests that were conducted. Chapter 3 gives description of various raw materials utilized for the project and also describes experimental methods in detail. The research focuses on the very early stages of reaction, during first 24 hours after mixing. The ultrasonic wave reflection method was used to study the setting and hardening behavior of cement pastes in the past and it has been extended to study geopolymer systems in this study. Shear wave reflection allows detection of the hardening process as decreasing wave energy reflects back to transducer with the development in the microstructure leading to stiffening[1]. The early age properties and strength development were studied using ultrasonic wave reflection method (UWR), Proctor penetration test and semi-adiabatic calorimetry which will be discussed in chapter 4. The microstructural development was studied using SEM-EDS analysis. The geopolymer solids were characterized using XRD and FT-IR techniques along with selectively dissolving products as discussed in chapter 5. Chapter 5 will also briefly discuss the characterization of pore solution extracted from geopolymer at various times and problems faced during the process. Conclusions are presented in chapter 6 followed by research output in chapter 7. References are provided in the end.

Chapter 2

Literature Review

2.1 Introduction

In 2007, nearly half of the electricity in United States was generated by coal and this process generated 130 million tons of flyash[6]. While 43 percent of this flyash was used beneficially, nearly 75 million tons was disposed of in engineered surface impoundments and landfills or in abandoned mines and quarries[7]. The release of radioactive minerals from flyash has significant impact to humans, wildlife and ecosystems. Contamination of ground water poses threat to the health of local communities when flyash is disposed in wet ponds. Therefore, it is important to develop technologies to utilize flyash into added-value products. One successful alternative would be to utilize flyash in the production of geopolymers. Geopolymers are environmental friendly materials with properties comparable to that of Portland concrete.

2.2 Geopolymer

Geopolymers are defined as amorphous to semi-crystalline three dimensional silico-aluminate structures of the Poly(sialate)type (-Si-O-Al-O-) or of the Poly(sialate-siloxo) type (-Si-O-Al-O-Si-O) by Davidovits[8]. The sialate network consists of SiO_4 and AlO_4 tetrahedra linked alternatively by sharing all the oxygens. Positive ions (Na^+, K^+, Li^+, Ca^{2+}) which are present in the framework cavities balance the negative charge of Al^{3+} in IV-fold coordination. Poly (sialates) are described by the following empirical formula:

$$M_n(-(SiO_2)_z\text{-}AlO_2)_n,\ wH_2O$$

Where "Z" is 1, 2 or 3; M is a monovalent cation such as potassium or sodium, and "n" is a degree of polymerization. Geopolymers are formed

by the polymerization of individual aluminate and silicate species, which are dissolved from their original sources at high pH in the presence of alkali metals. Much of research on geopolymers has focused on the use of potassium and sodium ions for activation and very little research on how other alkali and alkali earth cations, including calcium will participate in the reactions.

2.2.1 Advantages and Disadvantages

Utilization of flyash in producing geopolymer binders may result in environmental benefits such as reduction in use of natural resources, decrease in net production of CO_2 and mitigation of heavy elements leaching from the ash into soil from landfills[3, 9]. The other advantages are high compressive strength, fire resistance, and excellent resistance to sulfate attack, good acid resistance, low creep and minimal drying shrinkage[3].
The primary disadvantage is the use of chemical ingredients in the water for activation that might be corrosive to handle. This requires several safety procedures like using gloves, glasses and masks while handling them on-site. These might prohibit the use of geopolymers in mass applications. On the other hand, Portland cement or hydrated lime is typical mass products and geopolymer ingredients to be made user-friendly to compete with the popularity of Portland cement.

2.3 User-friendly Geopolymer

The Material Safety Data Sheets classify geopolymeric alkaline elements into two categories: corrosive products and irritant products. For the geopolymerisation, common practice is to use corrosive products where MR SiO_2:$M_2O \leq$ 1.45. These solutions are equivalent to concentrated alkaline hydroxide solutions and dangerous to work. To use them for regular building and civil engineering operations, where mostly people work with bare hands is not recommended. Davidovits had conceived the idea of user-friendly geopolymer where the alkaline activator is considered merely irritant (MR SiO_2:$M_2O \leq$ 1.45)and not corrosive. Normally, curing of flyash-based geopolymeric matrices is done at temperatures between 60 and 90^0C. Since, the idea was to use geopolymer as common cement; samples were cured at room temperature.

The use of Class C flyash requires high alkalinity in order to prevent flash setting during mixing. It is especially for flyash based geopolymers that high alkalinity is needed. Fly ash based geopolymers show good mechanical strength and durability. The limiting factor which has hindered the use is its low reactivity, which often leads to slow setting and strength development. The dissolution of fly ash is not complete before the final hardened structure is formed. To overcome the problem of low reactivity, slag is added to the system[10]. However, the use of slag+class F flyash mix along with potassium based activator allows the fabrication of flyash-based geopolymer with non-corrosive conditions in a user-friendly system.

2.3.1 Activator

It is generally accepted that Na is more effective in promoting aluminosilicate dissolution than K[11]. However, Davidovits[3] states that the fresh Na-containing geopolymers have greater yield stress than the K-containing geopolymers. This means that the Na-containing geopolymers are more viscous and harder to mix. It has also been proven that the compressive strength of K-geopolymers is higher than the Na-geopolymers. Tests have also shown that the higher amount of Na solution (50 % by weight) is needed to achieve same strength with K solution. This makes K-based geopolymers more user-friendly than Na-based geopolymers. In this present research, a combination of potassium silicate and potassium hydroxide is used as an activator.

2.4 Characterization

Geopolymeric compounds are either crystalline or non-crystalline (amorphous or glassy structure). Crystalline compounds result from hydrothermal setting conditions, whereas hardening at ambient temperature induces amorphous or glassy structures[3]. This thesis mainly focuses on user-friendly geopolymers which are cured at ambient temperature which results in amorphous structure. Classic characterization techniques like x-ray diffraction (XRD) give a broad halo rather than sharp diffraction peaks for such materials. Therefore, their structure cannot be investigated from XRD alone. Advanced techniques like Fourier transform infrared spectroscopy (FT-IR)

and Nuclear magnetic resonance (MAS-NMR) spectroscopy in conjunction with XRD to provide better insight into the molecular framework. XRD and FT-IR are used in the present study and discussion is permitted to those two techniques.

2.4.1 X-ray Diffraction

Geopolymer binders, like calcium silicates are obtained from hydration of Portland cement which are x-ray amorphous. In amorphous state, diffraction of x-rays results in a broad diffuse halo rather than sharp diffraction peaks. Early characterization studies on geopolymers have revealed that the geopolymers have a diffuse halo peak at about 3.05-3.30 Å (27-29$^0 2\theta$max, Cu Kα)[12]. Very often, the aluminosilicate raw materials contain small amounts of highly crystalline phases like quartz, corundum, titanium oxide, hematite, mullite etc. These phases provide strong reflection in x-ray diffractograms and care should be taken not to assign these with geopolymers. It was observed in one of the studies conducted with varying sodium content (0 to 50%) that the halo in the corresponding XRD patterns shifts to higher 2θ max with the increasing Na_2O content. Geopolymer products can be assumed to be amorphous equivalents of the major crystalline framework silico-aluminates.

2.4.2 FT-IR Infrared Spectroscopy

FT-IR is increasingly used for studying aluminosilicate materials including clay mineral. Several studies report spectra on zeolitic minerals, geopolymers and geopolymeric precursors. Most of these studies concentrate on the main (Si, Al-O) band which is around 1000 cm^{-1}. As the Si:Al ratio decreases, that is with higher Al inclusion, the wavelength of the main band shifts to lower wavenumbers. Spectra is seen to be plotted in both transmittance and absorbance mode. The IR spectra of geopolymers and precursors consist of the strongest vibrations found in all aluminosilicates, which are assigned to internal vibrations of Si-O-Si, Si-O-Al and are found at 950-1250 cm^{-1} and at 420-500 cm^{-1}.

2.5 Preliminary Studies

Preliminary studies on flyash-slag geopolymer were conducted with SiO_2/Al_2O_3 ratio of 1.25. The ratio was chosen based on the principal of user-friendly geopolymer where $SiO_2/Al_2O_3 \geq 1.25$ for the activator to be irritant and not corrosive to handle. Water to solids ratio was kept constant at 0.32. The mix was chosen based on the basis of the mix design by Davidovits[3, 5]. For determining the workability of geopolymer pastes, various ASTM standards were adopted. ASTM C 1437-07, a standard flow table test for hydraulic cement mortars was used to determine the workability of geopolymer pastes. The geopolymer paste was thixotropic and agitation due to flow table was resulting in wrong estimation of the workability. Assuming that mixes were very flowy, mini-slump cone method which is used for self-compacting cement mixes was adopted to determine the workability. But the paste was too viscous for the mini-slump cone method. Therefore, the cone with the following dimensions was used to determine the workability of all the mixes.

1. Height: 136.5mm
2. Bottom inner diameter: 165.1mm
3. Top inner diameter: 12.7 mm
4. Thickness: 6.35mm
5. Angle of the cone: 60^0

The cone was filled in three levels and was tamped 20 times with the tamper every level. Once the cone was completely filled, extra paste was cut off to a plane surface on the top of the cone. The cone was lifted one minute after the mixing operation and the diameter of the flow was measured after the flow was stopped (30 seconds). The diameter was measured using vernier calipers in four different directions and reported value is an average of these four readings. To understand the effect of slag, flyash and slag were added in different ratios and tested for workability and strength. Table 2.1 gives workability and strength values of various geopolymer mixes with varying slag content. Flow diameter of cement paste of similar w/c ratio is given for reference. Table 2.1 gives the indication that workability decreases with

Table 2.1: Workability and strength of various geopolymer mixes

Mix(14 day strength in MPa)	Diameter(cm)
Geo 0s(1.74)	23
Geo 5s(6.6)	22
Geo 10s(17.3)	19
Geo 15s(33)	16
Cement (w/c =0.35)	9.5

Geo 5s- 5% of slag by total weight

increasing slag content. On the contrary, there is a huge increase in compressive strength when the slag content was increased to 15% by total weight of the mix. This table illustrates a tradeoff between the ease of workability and the long term performance. Therefore, it is important to understand the reasons for hardening.

2.5.1 Effect of temperature

The user friendly geopolymer uses low concentration alkaline activator and room temperature curing. The effect of room temperature was observed to vary the chemical reaction considerably as shown in Figure 2.1. Two different room temperatures were chosen for the study, namely 22± 2 ^{0}C and 26±2^0 C. Raw materials were stored at room temperature and Geo 10s was chosen for the study. The chemical reaction was recorded by monitoring the temperature of the specimen using the semi-adiabatic calorimetry. Specifications of the experimental method will be described in chapter 3. From the Figure 2.1, when the outside room temperature and the initial raw materials were at 26^0 C, starting temperature was at 26.5^{0}C. The temperature rises until 28.5 ^{0}C in 30 minutes and stays almost constant at that temperature till 8 hours. A second peak appears at this time. On the other hand, when the outside temperature and initial raw materials were at 22^0 C, starting temperature recorded was 23.2^0 C. In this case, the temperature rises until 25^0 C in 1 hour and starts to decrease continuously for the next 16 hours. A second peak appears after this time. When the outside temperature was higher, the second peak appears earlier than otherwise. This

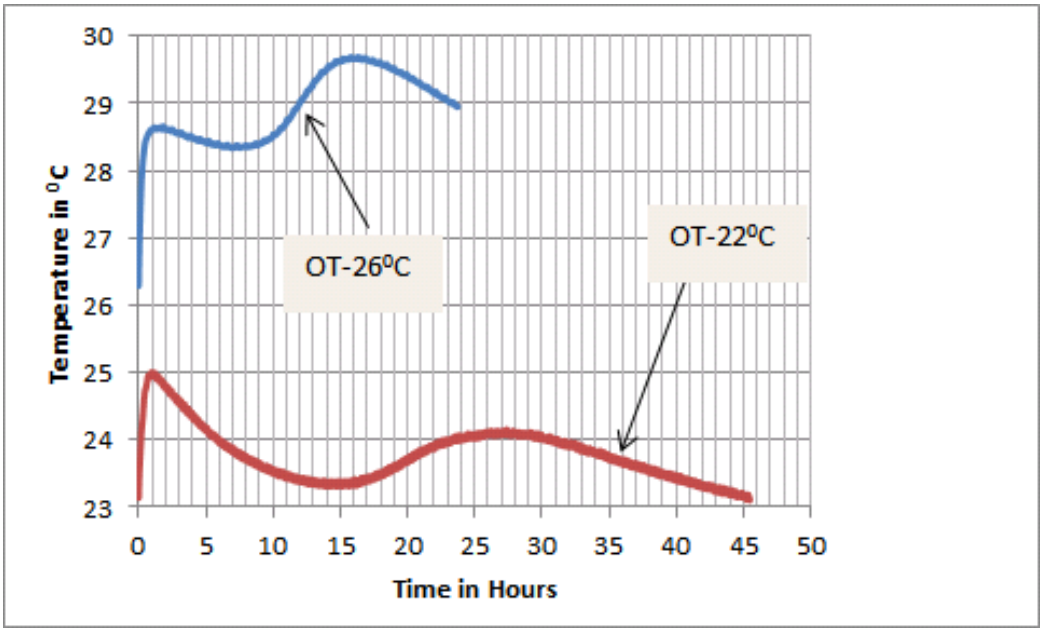

Figure 2.1: Effect of room temperature on the geopolymerisation

indicates that geopolymerisation has been higher in the case when outside temperature was higher. Temperature of raw materials and the outside temperature affect the geopolymerisation to a great extent. Interpretation of results would be fraught difficult if raw materials were stored at room temperature and when room temperature varies with seasons. Therefore, all the raw materials were stored at constant room temperature of 22 ± 2^0 C before the experiment. UWR and semi-adiabatic calorimetry were also conducted at the same temperature. Temperature of 22^0 C was chosen mainly based on convenience.

2.6 Effect of Calcium

Numerous studies have been carried out on systems with metakaolin mixed with various calcium sources. It has been found that various products, such as C-S-H gel, geopolymeric gel, Stratlinite and tetracalcium aluminium hydrate were formed. The coexistence of geopolymeric gel and calcium silicate hydrate was reported by various authors[13]. The percentages of different reaction products depend on various factors like alkalinity, ratio of aluminosilicate to calcium sources[14]. It was proven by authors that in a highly

alkaline environment, the alkaline activation of metakaolin in the presence of calcium hydroxide led to the formation of an amorphous sodium aluminosilicate, which has the same characteristics of geopolymeric gel. Davidovits in his patent on the method for obtaining geopolymeric binder allowing to stabilize, solidify and consolidate toxic and waste materials uses calcium to obtain a setting time equal to or greater than 30 minutes[15]. In this patent, it was described that the calcium ions determine the setting speed by making the alkaline geopolymeric gels less soluble. The optimal setting speed would be reached when the Ca^{2+} ions are integrated into the geopolymeric structure. The patent states that if the amount of alkaline Na^{+} or K^{+} is large, a large amount of Ca^{2+} ion will be necessary to obtain the same setting speed. Yet another study on metakaolin based geopolymers with various calcium silicate sources has revealed that the presence of calcium in any soluble form when added even in very small amounts has seen to be critical in early strength development[16].

On contrary, a very few studies were conducted on the flyash systems in the presence of calcium. In one of the studies, using flyash cements with 3-5% quicklime were reported accelerating of the hardening process and increase in compressive strength[17]. Addition of calcium has also known to significantly accelerate the setting and hardening of geopolymer, influencing the workability. The interaction between calcium, silicon and aluminate species is not well understood and has a significant impact on the type of reaction product and the behavior of geopolymer system in early ages [18, 19]. It is important to understand the role of calcium in optimizing the properties of user-friendly geopolmer systems.

The main objective of the present research was to study the early age properties of flyash-slag geopolymer and explore the microstructural and chemical changes responsible for the hardening. Having discussed the main reasons for hardening and stating the objectives of the present research, the first challenge was to monitor the hardening process. Vicat was used in some papers previously to study the setting behavior of geopolymers. Vicat and Proctor penetration tests were generally used on cement mortars for studying the setting behavior as well. But the main drawback with these methods is that the measurements are taken at discrete intervals possibly missing microstructural changes happening in between these measurements. Ultrasonic wave reflection method was chosen to measure the rate of hardening continu-

ously which resolves the problem at hand. A traditional Proctor penetration method was also performed along with semi-adiabatic calorimetry. Geopolymer solids were characterized using XRD and FT-IR. Subsequent chapters describe how these objectives are achieved.

Chapter 3

Experimental Procedures and Methods

The main aim of this thesis has been discussed in the previous chapters. Therefore, the present chapter is dedicated for detailed explanation of the raw materials and experimental methods adopted to achieve the specified objectives.

3.1 Materials

The main aluminosilicate materials used in this study were Class F flyash (a waste from coal industry) and Ground Granulated Blast Furnace Slag (GGBFS, waste from Iron industry). Flyash was provided by Boral Material Technologies and ground granulated blast furnace slag was supplied by Lafarge Corporation. The oxide composition of flyash and slag is listed in Table 3.1. The percentage of CaO by weight in flyash is 1.81% and slag is 39.4%. Since slag has very high percentage of CaO, for research purposes it is considered to be the only source of calcium ion. The particle distribution analysis of flyash and slag are given in Figure 3.2 and Figure 3.1. The mean size of flyash particles was $22.641\mu m$ and the mean size of slag particles was $14.024\mu m$.

The slag was added in various percentage replacements (0 to 15%) while keeping the total amount of powders constant. A combination of potassium silicate and potassium hydroxide were used to activate the aluminosilicate sources. Potassium silicate with solid content of 29% with SiO_2 = 20.75%, K_2O = 8.3% and modulus of 3.92 was produced by Pfaltz and Bauer and supplied by Fischer Scientific. Water to solids ratio was 0.32. Flyash, slag, silicates and potassium coming from potassium silicate and potassium hydroxide were considered as solids for calculating water to solids ratio. Potassium hydroxide crystals were dissolved in the extra water and mixed with

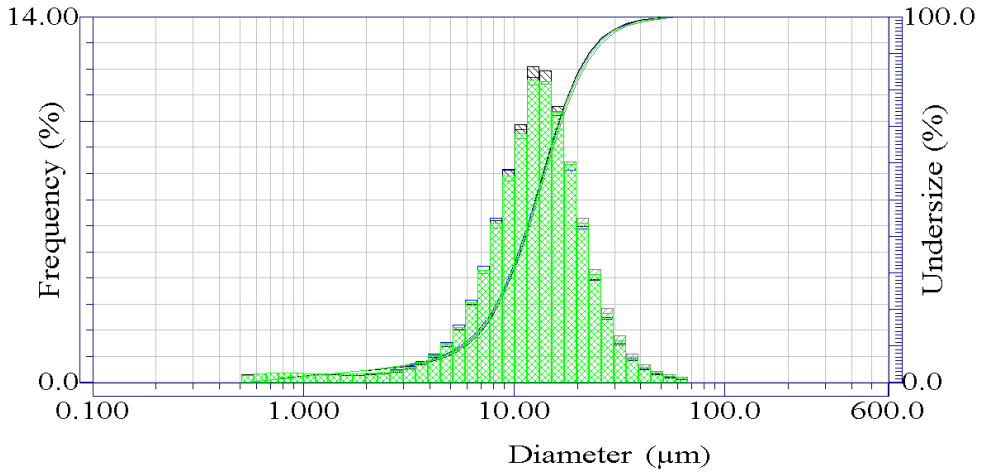

Figure 3.1: Particle size distribution of slag

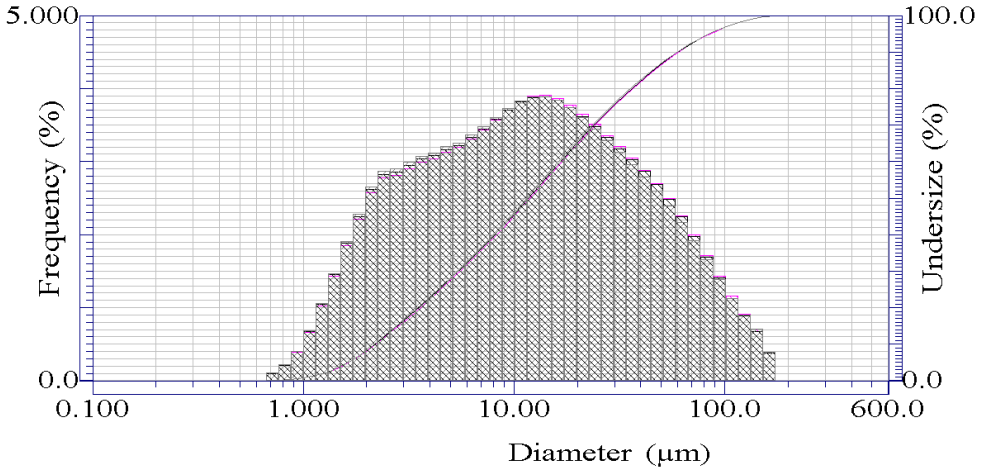

Figure 3.2: Particle size distribution of flyash

potassium silicate to a desired modulus. Different SiO_2/K_2O ratios, 1.25, 1.4 and 1.8 were tested to understand the effect of silicon to potassium ratio on the workability and compressive strength. Based on the properties, SiO_2/K_2O ratio of 1.25 was chosen for further studies.

Table 3.1: Oxide composition of raw materials used in the study (weight in %)

Composition	flyash	slag
SiO_2	60.17	35.7
Al_2O_3	21.91	11.21
CaO	1.81	39.4
Na_2O	0.81	0.26
K_2O	2.13	0.48
MgO	1.28	10.74
Fe_2O_3	7.57	0.42
SO_3	0.17	0.58

3.2 Mixing Procedure

The geopolymer was synthesized by mixing the flyash and slag with the activator solution. The activator solution was a mixture of potassium silicate and potassium hydroxide with $SiO_2/K_2O = 1.25$ and water. The water was added by calculating from water/solids = 0.32. Flyash and slag were mixed in different proportions by keeping molar ratio of $SiO_2/Al\ _2O_3$ constant at 5.1.

Class-F flyash and slag were weighed and the powders were mixed for 30 seconds at a speed of 104 RPM. The activator solution was added and mixed for next 3.5 minutes at the same speed. The reaction was observed to be sensitive to temperature and shear rate. To maintain the uniformity across the different tests, all raw materials were stored at constant temperature and 500 grams of material was mixed at constant shear unless otherwise mentioned.

3.3 Ultrasonic Wave Reflection Method (UWR)

Ultrasonic wave reflection (UWR) measurements were performed on various geopolymer pastes to monitor the rate of stiffening. A container with an approximate size of 50mm x 60mm x 50mm and thickness of 6.25 mm was used for UWR measurements. A container made from high impact polystyrene (HIPS) was used for UWR measurements. HIPS was chosen because it has

acoustic impedance very similar to that of cement paste thus providing sensitivity to small changes and it seems to work for geopolymers as well. Solid phenyl salicylate couplant was used to mount the transducer in the bottom of the HIPS buffer. The transducers were connected to two Panametrics 5077 pulser/receiver units. The pulser/receiver units were connected to a computer equipped with a NI 5102 PCI type digitizer (8-bit, 2 channel) using a sampling unit of 10 MHz for each transducer. The computer program, LabView was used to control, collect and process the data. Once the data was obtained, the wave reflection coefficient was calculated. The schematic diagram of UWR test setup is shown in Figure 3.3. Further details of this method can be found elsewhere[1]. The pulser/receiver units were switched on three hours prior to the testing with transducers attached to the buffer. After the geopolymer specimen was mixed, it was poured into HIPS buffer and the reflection coefficient was measured by using contact type 2.25 MHz s-wave transducers attached to the bottom of the container.
The cement mixture of w/c = 0.35 was used as reference for ultrasonic wave reflection. Shear waves (s-wave) and pressure waves (p-wave) were used to monitor the behavior of geopolymer mixes. The behavior of mixes obtained from s-wave UWR was compared with Proctor penetration method (ASTM C403). The rate of stiffening was monitored for 24 hours or till the complete debonding was seen. Debonding can be described as phenomenon where paste loses contact with the buffer material creating an air gap. The presence of air gap reflects all the shear energy which inhibits the measurement of any meaningful data thereafter.

3.3.1 Theory of Ultrasonic Wave Reflection

When a normal wave encounters a boundary between materials of different acoustic impedances, the wave is both transmitted and reflected at the boundary depending on the relative acoustic impedances of two materials. The two materials here are the hardening geopolymer paste and the buffer. The reflection coefficient at the boundary is given by

$$R = \frac{A_r}{A_t} = |\frac{Z_2 - Z_1}{Z_2 + Z_1}| \tag{3.1}$$

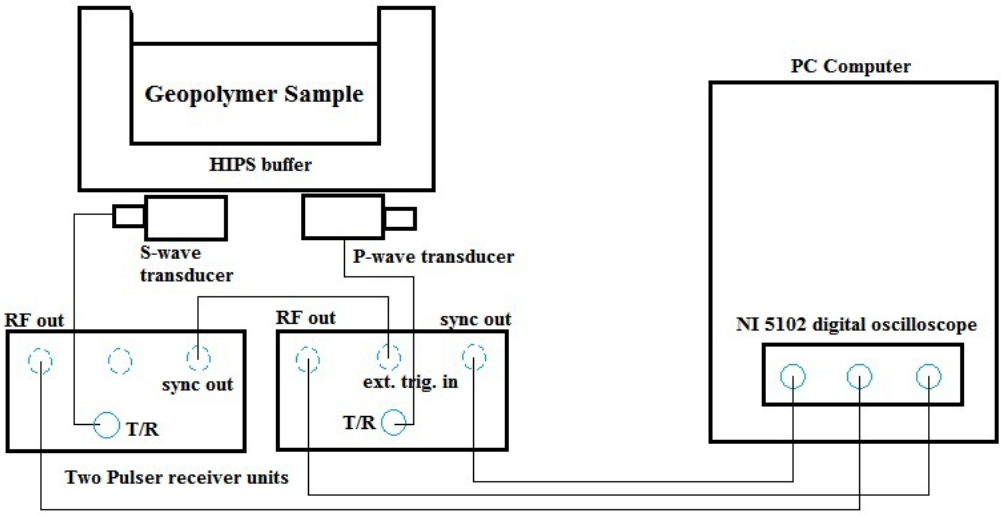

Figure 3.3: Schematic diagram of UWR test setup for geopolymer pastes[1]

Where R is the normal incidence reflection factor, A_r is the amplitude of the reflected wave, A_t is the amplitude of the incident wave, and Z_1 and Z_2 are the acoustic impedances of the buffer and test material, respectively[1]. The acoustic impedance ($Z = V \times \rho$) is defined as a product of velocity of the wave through the material, V and the density of the material, ρ. The acoustic impedance of HIPS buffer is close to that of the paste and that makes it sensitive to monitor small changes in the paste. When Z_1 and Z_2 become equal, no reflection will occur at this condition ($R = 0$) and this is called an inversion.

UWR method utilizes both incident shear waves (s-waves) and compression waves (p-waves). Shear waves can transmit through a solid, but not through a fluid. The wave is reflected completely in liquids and the s-wave reflection coefficient is unity. On the other hand, p-waves can transmit through both liquids and solids. As the geopolymer paste transforms from liquid to solid, the amount of shear wave transmitted increases and this decreases the reflection coefficient with time. Whereas p-wave UWR depends more directly on the difference in density between the buffer and the sample.

Traditional penetration tests like Proctor and Vicat measure strength at discrete intervals, whereas UWR is a continuous measurement, thus avoiding the possibility of missing the events between the discrete measurements. The

initial setting time and the final setting time for cement mortars have been traditionally determined from the Proctor penetration resistance. Recent developments have also facilitated the determination of setting times based on s-wave reflection coefficient. But the setting times for geopolymers are not determined in this study.

3.4 Proctor Penetration Test

Penetration resistance of geopolymer pastes was measured following the procedure in C403 using an Instron 4500 equipped with a 1 kN load cell. Penetration resistance was conducted mainly to monitor the stiffening behavior of various geopolymer mixes. Mixing procedure was same as described earlier except for the amount of the mix (2000 grams instead of 500 grams). After the sample was prepared, it was poured into a container of size 150 mm by 150 mm and poured to a depth of 50 mm. The container was tapped against a table three times to level out the paste and then covered with a moist towel to prevent evaporation of water. Time intervals at which penetration resistance measurements were made differed with mixtures largely depending on their UWR response. Measurements were started as early as five minutes after mixing and were taken every 5 minutes especially for mixes that set very rapidly. Six needles were used with cross sections of 645 mm^2, 323 mm^2, 161 mm^2, 65 mm^2, 32 mm^2 and 16 mm^2. Instron was programmed such that needles would penetrate to a depth of 25 mm in 10 seconds as prescribed in the code. Measurements were made starting with the needle of largest area and needles were changed as needed to provide the required penetration until the smallest needle was used. Change of needles was mostly based on tester's discretion with prior knowledge of rate of stiffening of various geopolymer pastes obtained from UWR measurements.

3.4.1 Calculation of Penetration Resistance

Penetration resistance was calculated by dividing the load with the area of the needle used for penetration.

$R = \frac{P}{A}$, where R is a penetration resistance, P is the load applied and A is the load bearing area of the needle used for penetrating to a depth of 25

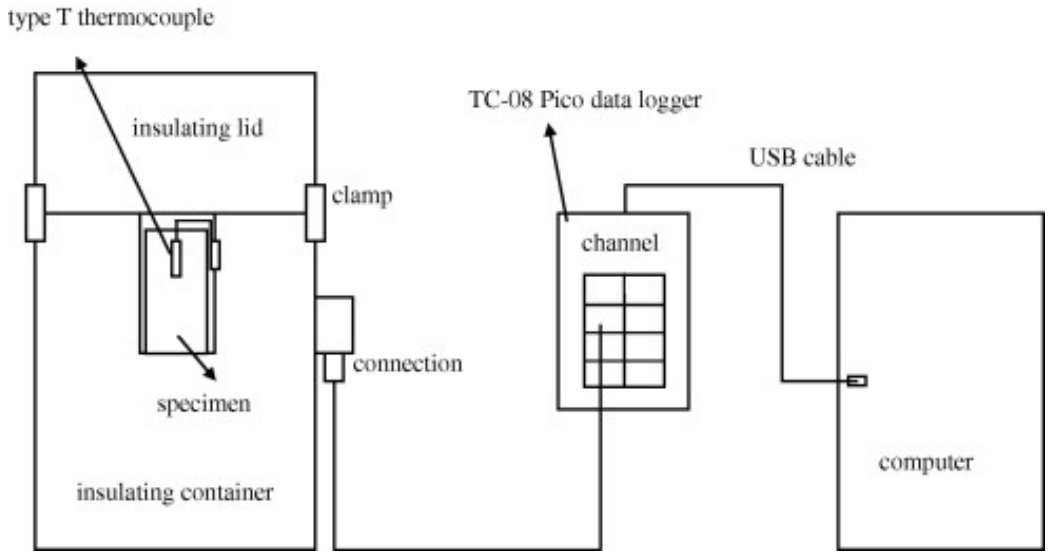

Figure 3.4: Schematic diagram of semi-adiabatic Calorimetry set up [2]

mm.

3.5 Temperature Measurement

To monitor the ongoing chemical reaction in various geopolymer mixes, semi-adiabatic calorimetry was used to track variation in temperature with time. Semi-adiabatic method uses a thermally insulated container and a type-T thermocouple to measure the temperature as a function of time. Since the environmental conditions are critical in case of semi-adiabatic calorimetry, the test was carried out in a climate controlled room at 21 ± 2^0C. A data logger was used to connect the thermocouple wire from the calorimetry container to the computer through a USB port. *Pico Logger* was the software used for data acquisition. After the sample was mixed, it was poured into the cylindrical container and placed into a thermally insulated calorimetric container. Type-T thermocouple which was soldered is inserted into the specimen and is connected to the container and data acquisition was started. Room temperature was also recorded along with the sample temperature. For recording the room temperature, soldered thermocouple was left open to the atmosphere and connected to the data logger. Schematic diagram of semi-adiabatic calorimetry is given in Figure 3.4

3.6 Microstructural Examination

The microstructural development responsible for hardening was sought to be determined through scanning electron microscopy (SEM). The development of microstructure was investigated by using the JEOL JSM-6060 LV SEM, equipped with energy dispersive x-ray spectroscopy (EDS). The electron source in the equipment was tungsten hairpin filament and operated under high vacuum mode. The microstructure of different samples at various ages was studied after treating them with acetone to stop the reaction. The fractured specimens were stored in a vacuum desiccator and were sputter coated with gold-palladium before imaging. After initial investigation, working voltage of 15 kV at probe diameter of 34 nm and working distance of 11 mm were determined as experimental parameters for achieving good quality micrographs at high magnifications. These were maintained consistently throughout the study unless stated otherwise. The mechanical preparation of flat-polished specimens for EDS analysis involved a series of grinding and polishing steps performed with progressively finer abrasives. After collecting a representative sample, first step would be to cast the sample in epoxy resin and was left for curing for at least 24 h. The impregnation was followed by very careful grinding and polishing to remove surplus epoxy and to create a plane surface of the specimen.

3.7 Phase Analysis

The composition of raw materials and various geopolymer samples was analyzed with XRD for various phases present. Careful, consistent sample preparation was necessary to obtain a representative, homogenous sample for analysis. A representative sample was chosen from geopolymer mixes at various ages and was flushed with acetone and finely powdered. Finely powdered sample was necessary to avoid preferred orientation, microabsorption, extinction, all of which can result in peak intensity errors. These ground samples were stored in a vacuum desiccator until XRD. Class F flyash had 86% of material pass through 45 sieve size, making it a very fine powder. Therefore it was not grinded any further for XRD. A glass sample holder of diameter 25mm and 1mm depth was chosen to ensure that there was large

enough surface for material under examination. X-ray diffractograms were recorded on a Siemens-Bruker D 5000 using a CuKα radiation at a voltage of 40 kV and current of 30 mA. Specimens were scanned from 5-70^0 2θ at 0.02^0 2θ steps and integrated at the rate of 1^0 min^{-1}. Positive phase identification can be made if at least three of the main diffraction peaks of the unknown match the standard diffraction pattern of a known crystal phase, which can be obtained from the literature of powder diffraction database. The software Jade 6.0 was used for basic analysis of XRD patterns. X-ray diffraction patterns of raw materials are given in the Figure 3.5, showing the main peaks of quartz, mullite and hematite in flyash. The broad amorphous hump in the XRD pattern, which is characteristic of flyash is seen ranging from 20^0 to 40^0 2θ. Slag is an amorphous glass, as evident from its XRD pattern with a hump centered around 30^0 2θ.

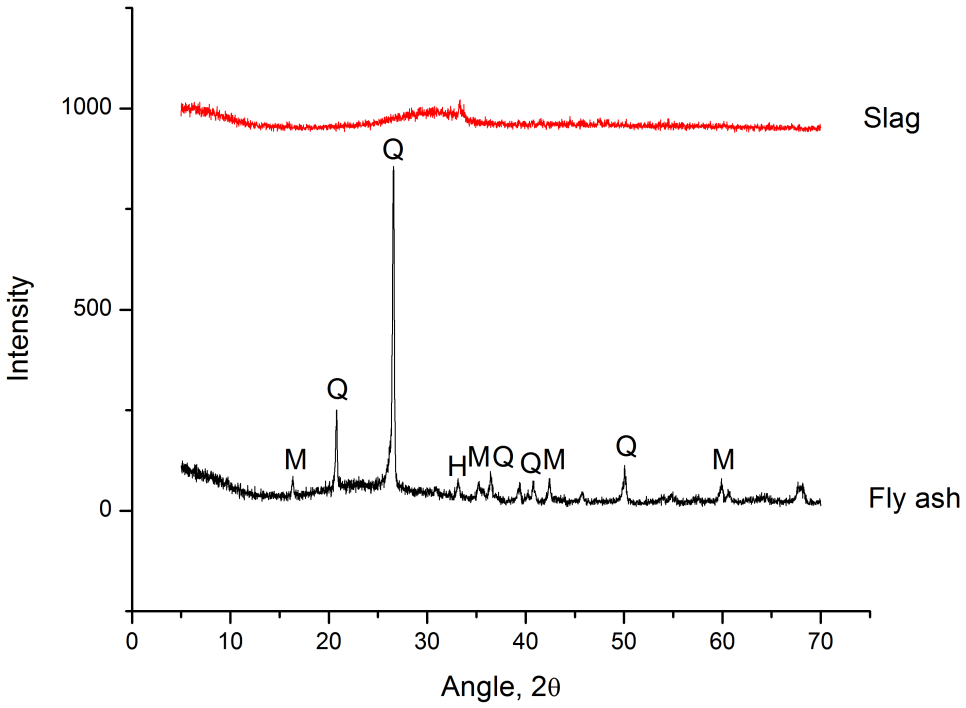

Figure 3.5: XRD pattern of raw materials (Flyash and Slag) where Q = Quartz, M= Mullite and H = Hematite. Broad amorphous hump centered at around 20^{0}2θ is seen in flyash and an amorphous hump centered around 30^{0}2θ is seen in the case of slag

3.8 Infrared Spectroscopy

3.8.1 Theory

When the external energy such as thermal or electromagnetic radiation is supplied, atoms get excited and vibrate about their equilibrium position. Like the energy associated with electrons, the vibrational energies of atoms are also quantized. This means a molecule can only absorb energy at some well-defined and discrete energy pockets called photons, which are characteristic of an individual molecule, or group of atoms. This is the basis for molecular identifications using a molecular vibration technique such as infrared spectroscopy (IR).

IR absorption spectrum is presented with wavelength or wavenumber on the x-axis and absorption intensity or percent transmittance on the y-axis. Transmittance, T, is the ratio of radiant power transmitted by the sample (I) to the radiant power incident on the sample (I_0). Absorbance (A) is the logarithm to the base 10 of the reciprocal of the transmittance (T).

$$A = log_{10}(\tfrac{1}{T}) = -log_{10}(T) = -log_{10}(I/I_0)$$

The transmittance spectra can provide better contrast between intensities of strong and weak bands because transmittance ranges from 0 to 100% T whereas absorbance ranges from infinity to zero. Samples were analyzed for both transmittance and absorbance spectra in the present study. Wavenumbers corresponding to infrared region ranges from 13000 to 10 cm^{-1}. The IR region is divided into three smaller regions: Far IR, mid IR and near IR. Mid IR region between 4000 to 400 cm^{-1} is frequently used because of the presence of fundamental vibrations of most molecules.

At temperature above absolute zero, all atoms in a molecule are in continuous vibration with respect to each other. When the frequency of a specific vibration is equal to the frequency of the IR radiation directed on the molecule, the molecule absorbs the radiation.

Each atom has three degrees of freedom, corresponding to motions along any of the three Cartesian coordinate axes. A polyatomic molecule of n atoms has $3n$ total degrees of freedom. However, 3 degrees of freedom are required to describe translation of the entire molecule and another 3 degrees

of freedom correspond to rotation of the entire molecule. Therefore, remaining $3n-6$ degrees of freedom are true fundamental vibrations for non-linear molecules. Linear molecules possess $3n-5$ fundamental vibrational modes. Among those $3n-5$ or $3n-6$ fundamental vibrations, those that produce a net change in the dipole moment may result in an IR activity.
From quantum mechanics, it is known that the oscillating dipole moment is an emitter or absorber of energy. The dipole moment produces oscillating electric field and if the frequency of that electric field matches with the oscillating electric field of the radiation, then the radiation is absorbed. So, when the energy is given to the molecule, molecule vibrates. When the frequency of dipole moment oscillation matches with the frequency of the IR spectrum then that particular frequency will be absorbed. Hence, molecules without a center of symmetry, which is normally the case in large molecules or amorphous solids, should be infrared active but Raman inactive. This is the reason why the infrared spectroscopy has been chosen over the Raman technique to characterize the nature of the geopolymeric products.
Vibrational frequencies observed in an infrared spectrum are dependent on

- The force constants of chemical bonds which measure the strength of the intramolecular bonding
- The atomic masses and
- The molecular geometry

In aluminosilicates, substitution of aluminum into a silicate structure has significant impact on the intramolecular bonding strength within an aluminosilicate. The Al-O bond in pure aluminate has a bond energy of 125 kJ mol^{-1} at the IV-coordination, whereas the VI-coordination, the Al-O bond energy is 87 kJ mol^{-1}. Compared to that of the Si-O bond of a pure silica with a bond energy of 466 kJ mol^{-1}, the Al-O bond clearly has a smaller bond strength regardless of the coordination state. A silica gel without any Al substitution or any other impurities is known to exhibit an IR asymmetric stretching Si-O-Si band centered at 1100 cm^{-1}. The IR asymmetric stretching bands of Al^{IV}-O-Al^{IV} and Al^{VI}-O-Al^{VI}, however are clearly situated at lower frequencies. With increasing aluminum substitution for silicon-rich aluminosilicates, the Si-O-T (T = Si or Al^{IV}) asymmetric stretching vibration band has been observed to shift from the original 1100 cm^{-1} to a lower

frequency indicating reduced average vibrational force constants resulting from decreased intramolecular bond strengths. Infrared spectrum was done in both transmission and absorption mode and results are presented in one of the ways.

Table 3.2: The characteristic IR vibrational bands of T-O-T(T= Si or Al) asymmetric stretching vibrations

W(cm^{-1})	Assignment
1100-900	Assymetric stretching(Si-O-Si, Si-O-Al)
1100-1000	Assymetric stretching(Si-O-Si, alkali catio-modified silicate)
1100	Assymetric stretching(Si-O-Si, pure silica)
900-650	Assymetric stretching(Al-O-Al, $Al^{IV}O_4$ tetrahedra, pure aluminate)
680-400	Assymetric stretching(Al-O-Al, $Al^{VI}O_4$ octahedra, pure aluminate)

$$W = Wavenumber$$

3.8.2 Transmission Spectrum

Fourier-transform infrared (FT-IR) spectra of powdered samples were acquired using a Thermo-Nicolet nexus 670 FT-IR spectrometer in transmission mode within the frequency range of 4000-800 cm^{-1} at a resolution of 4 cm^{-1}. The desired sample of amount 0.5 mg was mixed with 250 mg KBr and pellets were pressed to prepare infrared transparent matrix. Omnic is the software used for the IR. Liquid Nitrogen is used to purge the equipment and remove the CO_2 and H_2O which potentially interferes with the spectrum. Sample spectrum was collected after collecting the background spectrum. Software subtracts the background spectrum from the sample spectrum every time to remove bands coming from any environmental CO_2 and H_2O.

3.8.3 Absorption Spectrum

Thermo Nicolet Nexus 670 Fourier transform infrared spectrophotometer was used in absorption mode to acquire spectra. Golden gate attenuated total

reflectance accessory (ATR) with diamond crystal was used. The frequency range was from 4000 to 525 cm^{-1} at a resolution of 4 cm^{-1}. The spectrum was very noise below 700 cm^{-1}. A small amount of powdered sample was used to collect the spectrum. Sample was placed on the detector and a spectrum was collected. Liquid Nitrogen is not used in this mode. Spectral subtraction for environmental CO_2 and H_2O were done as described in the previous paragraph.

One of the advantages using ATR accessory was that there was no sample preparation. ATR works on the principle of total internal reflection in a crystal and the resulting evanescent wave. IR radiation passing through a crystal of higher refractive index reflects internally in a medium of higher refractive index if angle of incidence is greater than the critical angle. Although the beam is confined to the crystal, electromagnetic field of photon extends through the interface into the optically rare medium at the point of contact. The electrical field of the photons extends perpendicular to the beam direction and decays exponentially with distance from the surface of the optically dense medium. The field that extends from the surface into the optically rare medium is referred to as evanescent wave. The strength of evanescent wave decreases with distance into the optically rarer medium, sample in this case. The decay rate depends on the wavelength of the radiation, the refractive index of the crystal and the angle of incidence. The depth of penetration is typically 0.5-5 μ. Therefore, the amount of material is immaterial as along as good contact is established between sample and the crystal.

3.8.4 FT-IR of raw materials

Figure 3.6 gives IR spectrum of raw materials, flyash and slag. Flyash has a peak centered at 1050 cm^{-1} and slag on the other hand has a very broad peak, centered at 905 cm^{-1}.

3.9 Salicylic Acid-Methanol Extraction (SAM)

The presence of calcium silicate hydrate was predicted to cause rapid hardening in geopolymer samples. Since C-S-H was amorphous and hard to distin-

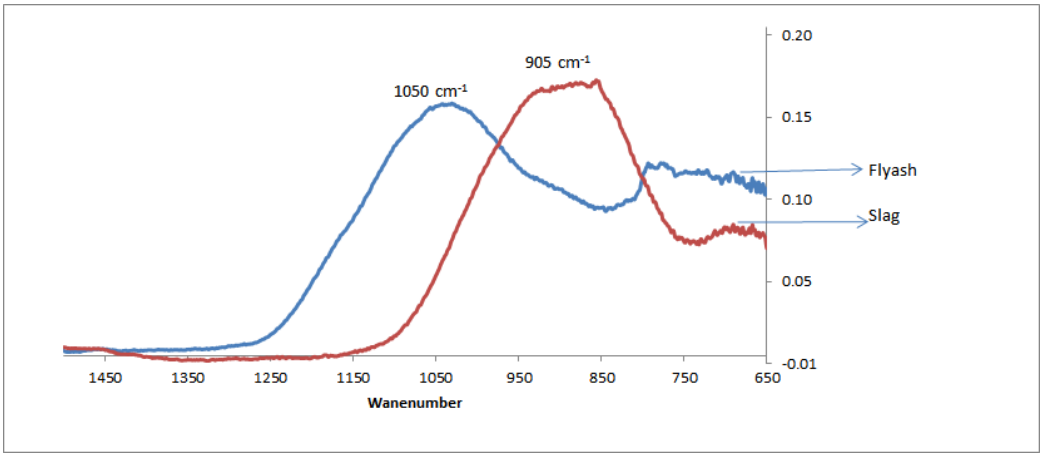

Figure 3.6: IR spectrum of raw materials, flyash and slag

guish it from other possible phases, salicylic acid/methanol (SAM) extraction was performed on the samples collected at various ages. For SAM extraction, 1 g of geopolymer sample was added to a solution containing 9 grams of salicylic acid mixed in 35 ml of methanol[20]. The mixture was stirred for 2 hours and the suspension was vacuum filtered using a Buchner funnel and a Whattman filter. Insoluble residue was washed with methanol and stored in vacuum desiccator until analysis. X-ray diffraction and Fourier transform Infrared analysis (FT-IR) were done on these specimens to observe changes after the treatment.

Spectrum(C-S-H) = Spectrum (Unreacted flyash+Geopolymer+C-S-H) - x*Spectrum (Residue after SAM extraction containing Unreacted flyash+Geopolymer)
C-S-H:Calcium Silicate Hydrate, SAM: Salicylic acid - Methanol, x: amount of insoluble residue left after treatment per 1 gm of initial material

3.10 Determining the Amount of Geopolymer Product Formed

Geopolymer is an amorphous aluminosilicate product. Conventional techniques used for characterizing cementitious products like XRD cannot be used in the case of amorphous geopolymer products. This poses severe limitation to the characterization of product. More advanced techniques like Fourier transform infrared spectroscopy (FT-IR) technique should be used

to probe amorphous products. Primary interest of the present research was to investigate reasons behind rapid hardening of flyash geopolymers when slag was added. However, results have indicated that considerable amount of flyash remains unreacted at early ages rendering the FT-IR spectra difficult to interpret. One of the methods proposed by Palomo et al.[21] was to selectively dissolve the product formed and subtract the spectra of unreacted flyash from the total spectra to obtain the spectra of geopolymer product as given in the equation below. Spectrum (Geopolymer) = Spectrum (Unreacted flyash+Geopolymer+C-S-H) - y*Spectrum (Residue after HCl treatment containing unreacted flyash+silica gel) *y: amount of insoluble residue left after treatment per 1 gm of initial material* The selective dissolution process includes treating the hardened paste with 1:20 HCl (by volume). Attack with acid provokes dissolution of the chief reaction product of alkali activated flyash (aluminosilicate gel and zeolites) leaving behind the unreacted ash as insoluble residue. As described elsewhere,[22] the experimental procedure consists of adding 1g of activated flyash (flyash and slag in this case) to a beaker containing 250ml of (1:20) HCl. The mixture was stirred for 3 hours followed by filtration. Insoluble residue was washed with de-ionized water several times to a neutral pH. The insoluble residue was dried at 100^0C and then stored in the vacuum desiccator till the analysis was done. It was not calcined at 1000^0C as described in the procedure[22]. Calcination at 1000^0 was a necessary step for calculating the exact amount of product dissolved, since it is important to measure the weight of the powders before and after the treatment that are similar in their state in terms of moisture content. Since the primary interest was just to dissolve the reaction products for determining them using FT-IR, calcination was avoided largely based on convenience. The trials were repeated at least three times to guarantee reproducibility.

Acid treatment dissolves geopolymer product and zeolites and also effects calcium silicate hydrate (C-S-H). Under acid attack, calcium silicate hydrate decomposes with removal of Ca^{2+} leaving silica gel behind[23]. The peaks of silica gel in FT-IR spectrum might coincide with those in the original geopolymer product which should not be forgotten during the analysis.

3.11 Pore Solution Analysis

The interaction between calcium, silicon and aluminum species might have significant impact on the type of reaction product and the behavior of geopolymer systems in early ages. Therefore, it is important to understand and relate the concentration of ions with the hardening behavior of the system obtained from UWR and Proctor penetration. To study the variation in ion concentrations with time, the pore solution was extracted at specific times and analyzed by Inductively Coupled Plasma - Optical Emission Spectroscopy (ICP-OES).

After the mix was prepared, a constant amount was poured into centrifuge vials. At a defined time, two vials were centrifuged at 1000 RPM for 15 minutes to extract the pore solution. Two vials of constant amount were used to keep centrifuge from shaking vigorously. After 15 minutes of centrifuging, the vials were removed and pore solution was extracted using syringe needle attached to Luer tip of a gastight glass syringe. A 1000 series gastight syringe of volume 1.0 ml, manufactured by Hamilton was used. A syringe filter with Polytetrafluoroethylene (PTFE) membrane of pore size $0.2\mu m$ attached to syringe needle was used to pierce through the vial cap without exposing it to the atmosphere. Extracted fluids were diluted immediately in distilled (DI) water acidified to pH 1.0 with nitric acid to neutralize the pH and prevent it from forming a gel. Volume and weight of pore solution was measured.

Syringe filter made from PTFE membranes were chosen because PTFE is resistant to high alkaline solution like the pore solution extracted from geopolymer samples. Appropriate care is needed to prevent contamination between the samples. A syringe should be flushed with approximately 5-10 times to eliminate carryover between samples. To avoid the contamination, distilled water (DI) should be repeatedly drawn and expelled from the syringe. Acetone should be used for cleaning only after rinsing with deionized water. When acetone was used to clean the syringe before using DI water, left over acetone in the barrel affected the PTFE membrane. Hence, care was taken not to clean the barrel with just acetone. It was always flushed later with DI water.

The ion concentrations (K, Si, Ca and Al) were analyzed by PerkinElmer Optima 2000DV ICP-OES in radial mode. Commercial NIST traceable standards at 1000ppm, were diluted to the levels needed for analysis and all the

standards were built in 1% trace HNO_3. The following three different sets of standards were prepared:

1. Al was run undiluted, with a 1% HNO_3 blank and a 20ppm standard
2. Ca was run in a 1:10 dilution against a 20 ppm standard
3. K and Si were run in 1:50 dilution against a K-40ppm and Si-20 ppm standard

The instrument calculates concentrations taking the aliquot dilutions into consideration, so all the reported concentrations refer to the original solution (pore solution diluted in acid solution) and are given in terms of parts per million (ppm). Since volume and weight of pore solution are measured, values given in ppm are converted to moles per liter.
The method described here was finalized after several trials. Several attempts were made to avoid the exposure of pore solution to the environment. One of the attempts was to add the pore solution to acid in N_2 environment. Nitrogen environment was created by pumping nitrogen into a glove bag. Inside the glove bag, arrangements were made for vacuum filtration. Whattman filter paper No. 50 was used for filtration. Immediately after centrifuging, the solution was transferred into the glove bag through a specially made opening. Once the solution was filtered, it was transferred to the acid solution. The weight of pore solution was calculated and samples were sent for ICP-OES analysis.

Chapter 4

Hardening Rate of Geopolymer Pastes

Preliminary investigation on workability and compressive strength of flyash geopolymers has revealed that addition of small amount of slag influences the early age and later age properties of flyash geopolymers to a large extent. Hence, monitoring the stiffening rate of geopolymers in the early age will be critical for its use on site. Traditional methods like Proctor penetration and Vicat test were used to monitor the setting behavior and strength development in the case of cement pastes and mortars. The Vicat test uses only one needle and does not give information on progressive stiffening process. On the other hand, Proctor test is a more advanced technique where different sized needles are used to monitor gradual stiffening of mortars. The methods are simple and cheap, however, these tests give data at discrete times. Ultrasonic wave reflection method (UWR) has been developed to overcome difficulties with the above described methods and to continuously monitor the stiffening and setting behavior of cement mortars. The method has been extensively studied for cement pastes and mortars[1]. UWR has been used for the first time in this research to study the stiffening behavior of geopolymer pastes.

In this chapter, UWR (shear waves and pressure waves) is used to monitor the stiffening of geopolymer pastes and s-wave UWR is more emphasized throughout the chapter. Since, UWR is used for the first time to study geopolymer pastes; penetration resistance test (ASTM C 403) was used to understand the behavior of mixes. The temperature rise was also monitored to correlate stiffening characteristics.

The UWR and penetration resistance of cement paste of w/c ratio 0.35 will be described in the chapter prior to understanding the behavior of geopolymer pastes. The hardening rate and strength development with time of geopolymer pastes with varying slag replacements (0 to 15%) was investigated.

4.1 Normal Cement Paste

4.1.1 Ultrasonic S-wave Reflection

Ultrasonic wave reflection method was extensively used to study the setting and strengthening of plain cement pastes[1]. Reflection coefficient, $R(t)$ is calculated as described in the previous chapter. R(t) for cement paste with w/c =0.35 is given in Figure 4.1. The initial R(t) value is equal to one as s-waves do not pass through the initial fluid cement paste. A small drop in the reflection coefficient seen until first 20 minutes has been attributed to reflocculation of the cement paste after it has been poured into the container. Hereafter, there is roughly no change in the value of R during the induction period until 100 minutes. After the induction period, R(t) decreases rapidly until inversion. As described earlier in chapter 3, inversion is a point where paste and buffer have same acoustic impedances and after the inversion, as paste impedance continues to increase, R changes the direction and increases. R(t) value is still positive because of the use of modulus. The initial setting time has been defined as a time when R(t) value reaches a value of 0.83 and the final setting time has been defined as a time at inflection point in R(t). According to these parameters, the initial set time in this case is 160 minutes and the final set time is 220 minutes.

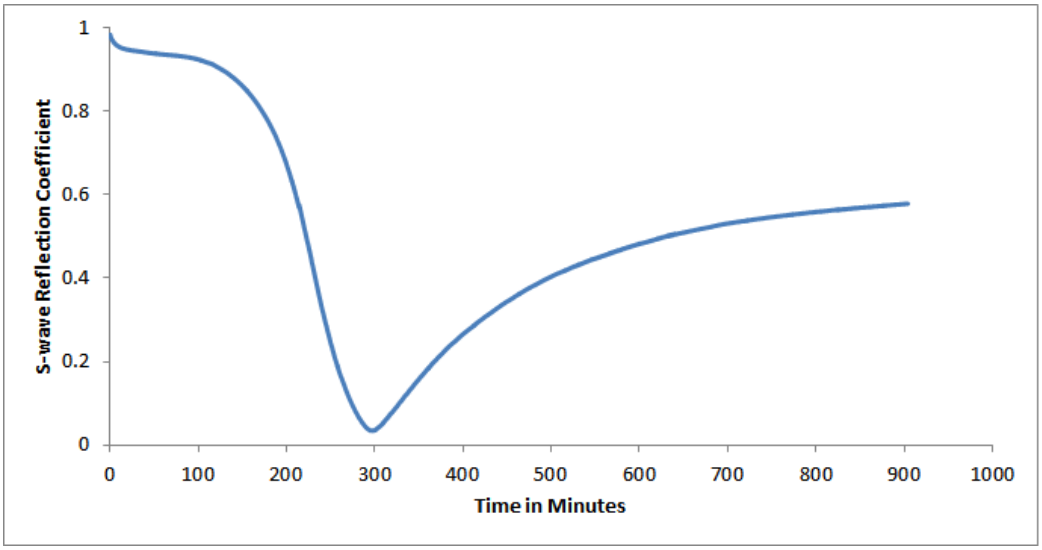

Figure 4.1: S-wave UWR behavior of cement paste (w/c =0.35)

4.1.2 Penetration Resistance of Cement Paste

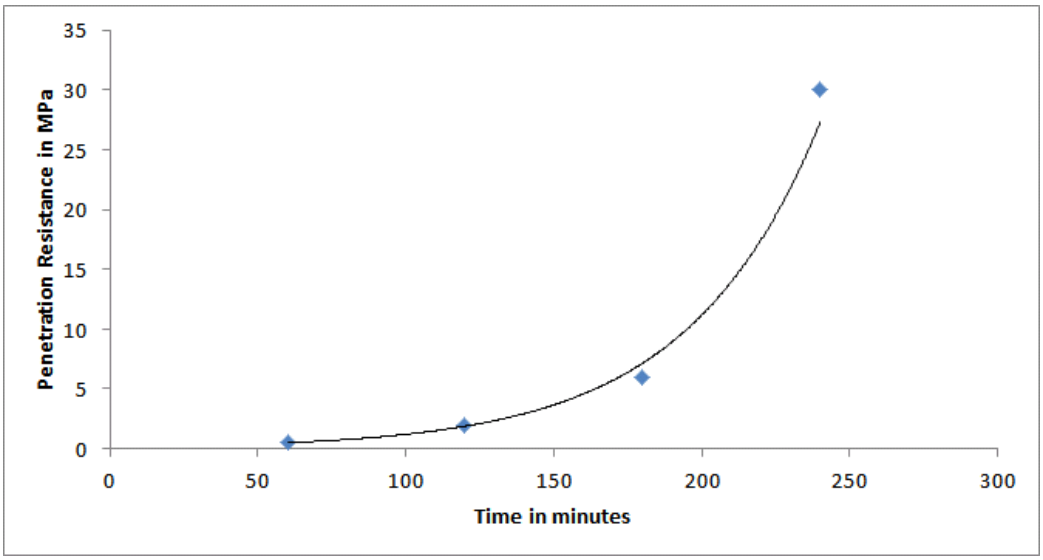

Figure 4.2: The penetration resistance of cement paste with w/c =0.35

A cement paste of w/c =0.35 (Figure 4.2) was tested for penetration resistance. The cement paste showed almost zero penetration rresistance until 60 minutes followed by an exponential increase. The measurements were taken every one hour and needles were chosen based on tester's discretion. The cement paste shows an induction period of approximately 100 minutes followed by an exponential increase in the penetration resistance. This response is very similar to that seen from UWR response. Exponential function was fitted to the curve. The initial and final set times were found as the times the fitted curve reached values of 2 MPa and 14 MPa, respectively. The initial set time and final set times for the cement paste from the curve are 120 minutes and 210 minutes respectively.

S-wave UWR and Proctor penetration tests were studied on cement pastes with different w/c ratios. Initial and final set times were found out from both the methods and compared. The relationship was found to be approximately linear and the correlation moderately strong. The validity of UWR method to determine the setting behavior was established[24, 1]. This method was further extended to study different systems like geopolymers for the present study.

4.2 S-wave UWR of Geopolymer Pastes

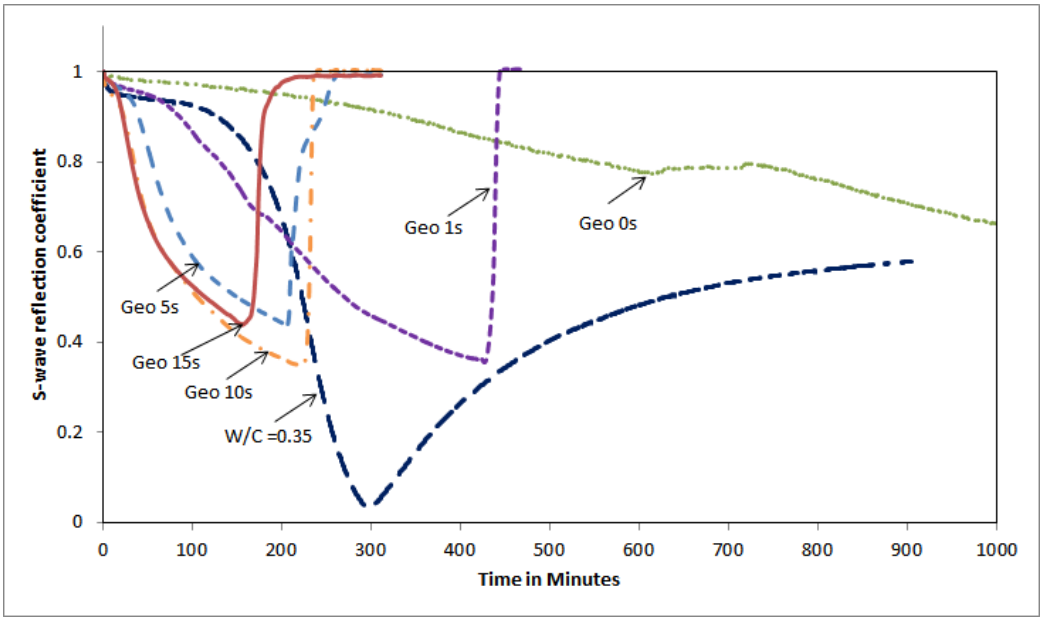

Figure 4.3: The change in s-wave reflection coefficient with time for flyash geopolymers with variable amount of slag (0, 1, 5, 10 and 15%). Notation: Geo10s, where 10 indicates the percentage of slag by total weight of the mix

Figure 4.3 presents the time vs. s-wave reflection coefficient plot for flyash geopolymers with varying slag content. The cement paste of water to solids ratio 0.35 was chosen as a reference to compare with geopolymer pastes of water to solids ratio 0.32. In case of Geo 0s (flyash geopolymer with 0% slag replacement), the rate of hardening is observed to be very slow as the s-wave reflection coefficient changes very slowly and remains roughly around 0.6 even after 1000 minutes. On the contrary, when 5% (by total weight) slag was added to the mix, the s-wave reflection coefficient drops rapidly for the first 70-80 minutes and more slowly thereafter. A rapid increase in the s-wave reflection coefficient is seen after 190 minutes, which is associated with complete debonding of the specimen from the buffer surface. Since, s-wave can be reflected completely by the air pocket/gap (at the interface between air and buffer material), the value of the reflection coefficient reaches 1. The occurrence of debonding was possibly due to drying of water or chemical shrinkage which limited the data collection from UWR. The behavior of Geo 10s and Geo 15s can be described in a similar manner. Debonding is not

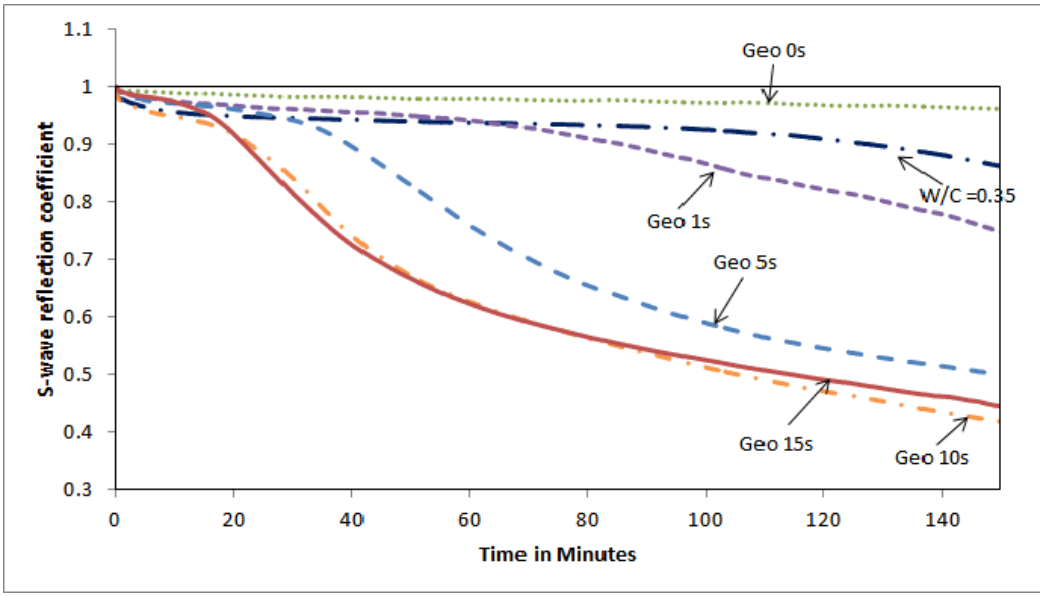

Figure 4.4: First 100 minutes of s-wave response. a: Cement paste (w/c=0.35), b: Geo 0s, c: Geo 1s, d: Geo 5s, e: Geo 10s, f: Geo 15s

observed in the case of Geo0s which indicates that there was no volume change of geopolymer that could be detected by UWR within the first 1200 minutes of reaction (time of experiment). In order to study differences in the rate of stiffening for different mixes, Figure 4.4 presents a close up of first 100 minutes. The times for onset of hardening for different geopolymer mixes (Geo 1s, Geo 5s, Geo 10s and Geo 15) as defined by onset of rapid drop in the reflection coefficient are 65 minutes, 30 minutes, 15 minutes and 10 minutes respectively. Clearly, as the amount of slag increases, the time for onset of hardening decreases. The changes in slope observed around 50-80 minutes indicates that the hardening rates are faster at the beginning and slows down thereafter.

4.3 P-wave UWR Response of Geopolymer Pastes

Figure 4.5 gives p-wave response of geopolymer mixes. P-wave UWR response is considered as a better measure for debonding since it is sensitive to the air gap at the interface of buffer and the specimen. P-wave reflection coefficient changes rapidly by a drop followed with a sudden increase which is due to complete debonding. Debonding times for Geo 15s, Geo 10s, Geo

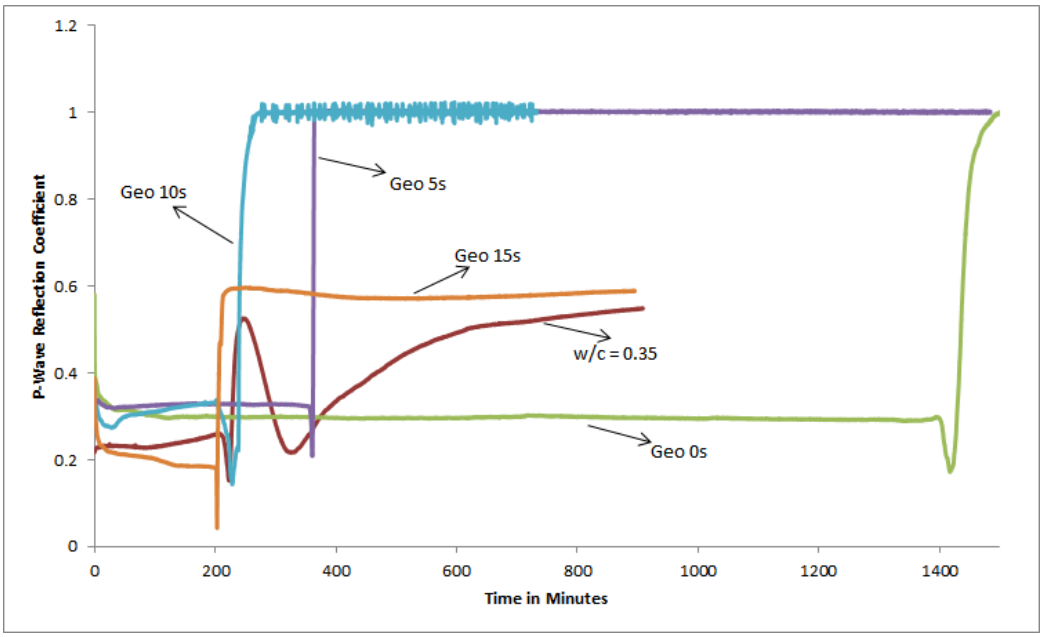

Figure 4.5: Change in p-wave reflection coefficient with time for flyash geopolymers with variable amount of slag (0, 5, 10 and 15%)

5s and Geo 0s are 175 minutes, 200 minutes, 300 minutes and 1380 minutes respectively. The debonding times follow a trend which is very similar to the hardening rates as determined by s-wave UWR. Considering that the environmental conditions are similar for all the mixes, debonding might have been caused by both chemical and drying shrinkage. Pursuant to Temuujin et. al.[25] the amount of shrinkage could be related to the presence of chemically bound water with the geopolymer gel and higher shrinkage may be an indication of insufficient geopolymerisation reaction. If the above theory holds then Geo 0s should have the earliest debonding which is not the case. Geo 15s with the maximum reaction rate is showing the earliest debonding and therefore highest shrinkage followed by Geo 10s and Geo 5s. So, shrinkage is not just related to drying of freely available water but also due to the formation of products.

4.4 Penetration Resistance of Geopolymer Pastes

A more traditional Proctor penetration test was performed to relate UWR response with the strength development. Figure 4.6 gives Proctor resistance

for all the mixes, plotted as a function of time. Geo 0s offers nearly zero resistance until 300 minutes after which the resistance increases slowly. This corresponds to s-wave reflection coefficient of nearly, 0.95-0.9. It can be concluded that the strength development was slow until 300 minutes after which resistance increases indicating strength gain. On the contrary, Geo 15s shows an increase in resistance from 5 minutes after mixing and increases rapidly till 80 minutes. This corresponds to the rapid drop in reflection coefficient as observed in UWR indicating rapid hardening/strength development. The slope of proctor resistance curve changes around 80 minutes, indicating the rate of strength gain has slowed down which again correlates well with UWR results which show a change in s-wave reflection coefficient. The behavior of other mixes follows a similar pattern as that of Geo 15s. Increase in Proctor resistance for Geo 1s, Geo 5s and Geo 10s starts at 70 minutes, 30 minutes and 10 minutes respectively after mixing, which corresponds well with the onset of hardening measured from UWR. It is important to note that as the amount of slag increases, the onset of proctor resistance is observed earlier. The initial and final setting times for geopolymers cannot be determined from UWR and proctor resistance by comparing it with results based on cement mortars. The two systems differ in the mechanism of hardening and further research is needed to relate microstructural changes with hardening. The hardening seen from UWR correlates well with the strength gain of the microstructure from proctor penetration test.

4.4.1 Semi-adiabatic Calorimetry

Semi-adiabatic calorimetry was used to measure temperature changes in different mixes during first 1000-3000 minutes after mixing. Temperature-time curves shown in Figure 4.7 give an indication of ongoing chemical changes. The temperature measurement was started within 30 seconds after mixing. In the case of Geo 0s, temperature decreases continuously and reaches room temperature (22^0 C) within 1000 minutes. On contrary, Geo 5s, Geo 10s and Geo 15s show initial rise in temperature and reaches a peak temperature within first 80, 30 and 15 minutes respectively. Temperature decreases thereafter, reaching room temperature within 1500 minutes in case of Geo 5s. Geo 10s and Geo 15s show a second peak and it appears sooner in case

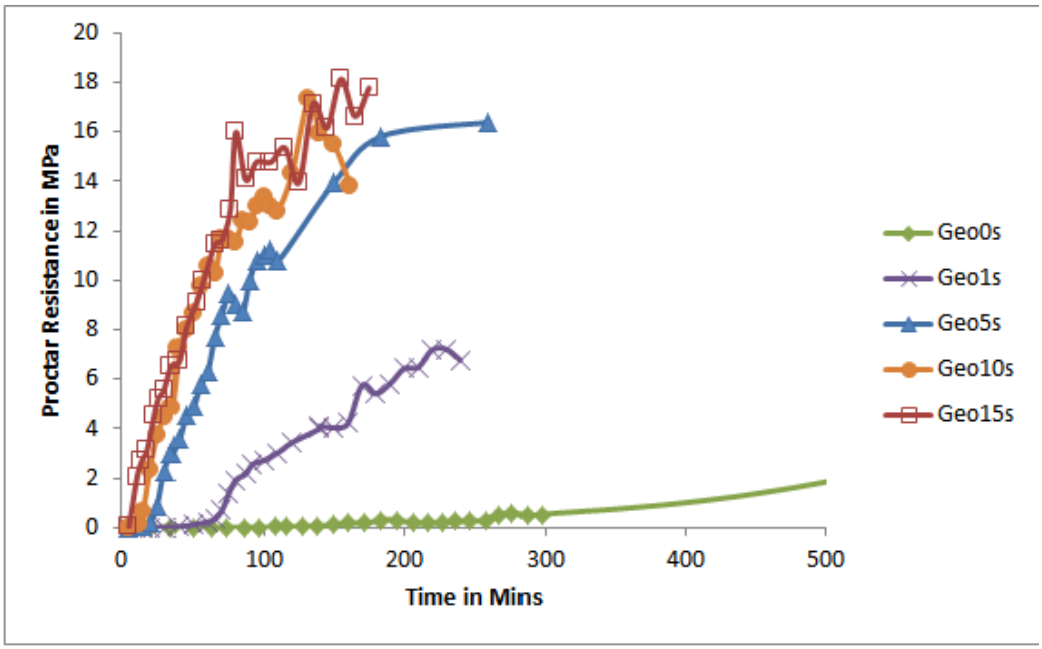

Figure 4.6: Proctor resistance of various geopolymer mixes showing the strength development

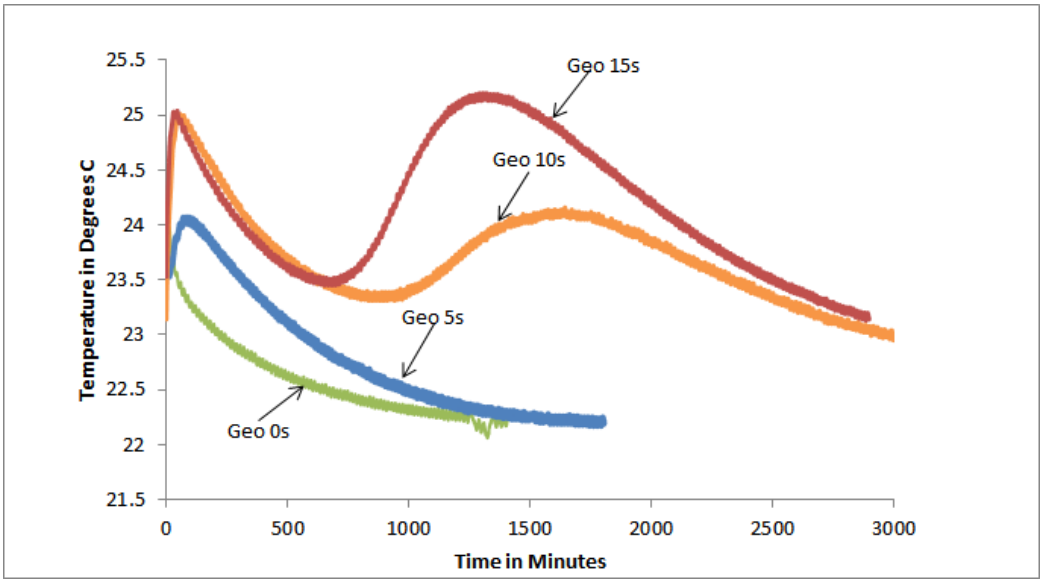

Figure 4.7: Temperature vs time curve for various geopolymer mixes obtained using semi-adiabatic calorimetry

of Geo 15s compared to Geo 10s. This second peak did not appear within the time frame of experiment for Geo 0s and Geo 5s. In the case of Geo 5s, the broad peak from 35 minutes to 100 minutes corresponds to the rapid hardening phase as detected by UWR. A similar behavior was observed in the case of Geo 10s and Geo 15s. As evident from calorimetry, the total temperature change is nearly 4^0 C which is much lower than that of cement paste. The low heat of reaction accompanied by strength development can be advantageous in the applications of geopolymers.

The present study employs UWR for the first time to study the hardening behavior of geopolymer mixes. Information obtained from UWR correlates well with more traditional measurement of stiffening behavior using proctor penetration test. For example, the decrease in s-wave reflection coefficient of flyash geopolymer was slow in the absence of slag indicating delayed hardening. Lower reaction rate and low strength development has been reported by other authors when flyash is activated with low alkaline activator concentration without heat curing[3]. This is also seen from proctor penetration results where the resistance to proctor penetration is 0 MPa for the first 300 minutes, indicating no significant strength development. Flyash geopolymer in the absence of slag has a continuously decreasing temperature curve (semi-adiabatic calorimetry) with time indicating that the initial temperature rise due to wetting was not followed by the product formation. Delayed hardening as indicated by UWR and proctor penetration test was related to slow development in the microstructure.

The increase in slag content by a small quantity shows an initial rapid drop in s-wave reflection coefficient and slowly thereafter. The hardening behavior of these mixes can be characterized under rapid hardening. The similar behavior was seen with proctor penetration test. Addition of small amount of slag rapidly changes the strength development of the microstructure. The proctor penetration shows an high resistance initially which slows down with time. Changes in Proctor resistance with time for all the mixes relate well with that of UWR results. Calorimetry curves for flyash geopolymers either show one peak or two depending on the amount of slag substitution. The decrease in the temperature after the initial peak may be assumed because of the decrease in the precipitation due to accretion of products on the flyash thus slowing down the reaction. The appearance of a second peak can be attributed to the second stage of precipitation which might have been initi-

Table 4.1: 14 day compressive strength of geopolymer mixes (0, 5, 10, and 15). The compressive strength was measured on 1-inch * 2-inch cylinders using Forney machine. The compressive strength values are average of three cylinders

Mix	Compressive Strength (MPa)
Geo 0s	1.4
Geo 5s	6.8
Geo 10s	17.4
Geo 15s	33.0

ated by ions reaching critical concentration. Therefore, drop in the s-wave reflection coefficient (hardening) can be directly related to the strength gain and the microstructural development.

As the percentage of slag increases, it was observed that the time for onset of hardening decreases (Figure 4.4,Figure 4.6) indicating that the hardening rate and the onset of hardening depends on the percentage replacement of slag. But the compressive strength increases with the amount of slag replacement given by Table 4.1. It is a compromise between compressive strength and workability.

Previous studies have reported accelerated hardening when calcium was added to flyash but for the first time, there is a clear and carefully monitored evidence of the hardening with time [26, 16]. Calcium dissolving from slag can be assumed to influence the hardening rate of flyash-slag geopolymers and also the reason for the appearance of second peak earlier in the case of Geo 15s compared to Geo 10s. It can be assumed that the calcium released from slag might be playing a critical role. The effect of calcium on the hardening still remains as a hypothesis.

4.5 Effect of Calcium on the Hardening Behavior

As calcium is known to alter hardening rate of geopolymer, the effects of slag as mentioned above can be assumed to be due to calcium coming from slag (as the Ca content of class F flyash used in this study is very low). To confirm this and to understand the effect of calcium more carefully, CaO

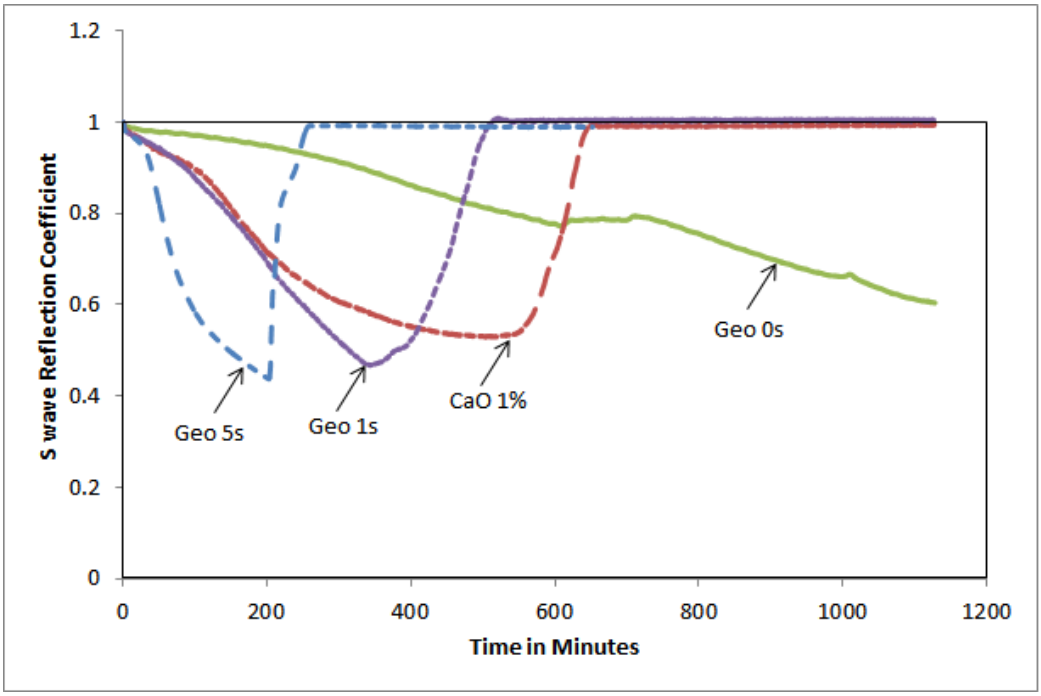

Figure 4.8: S-wave UWR of flyash geopolymers showing the effect of calcium on the hardening rate of flyash geopolymers

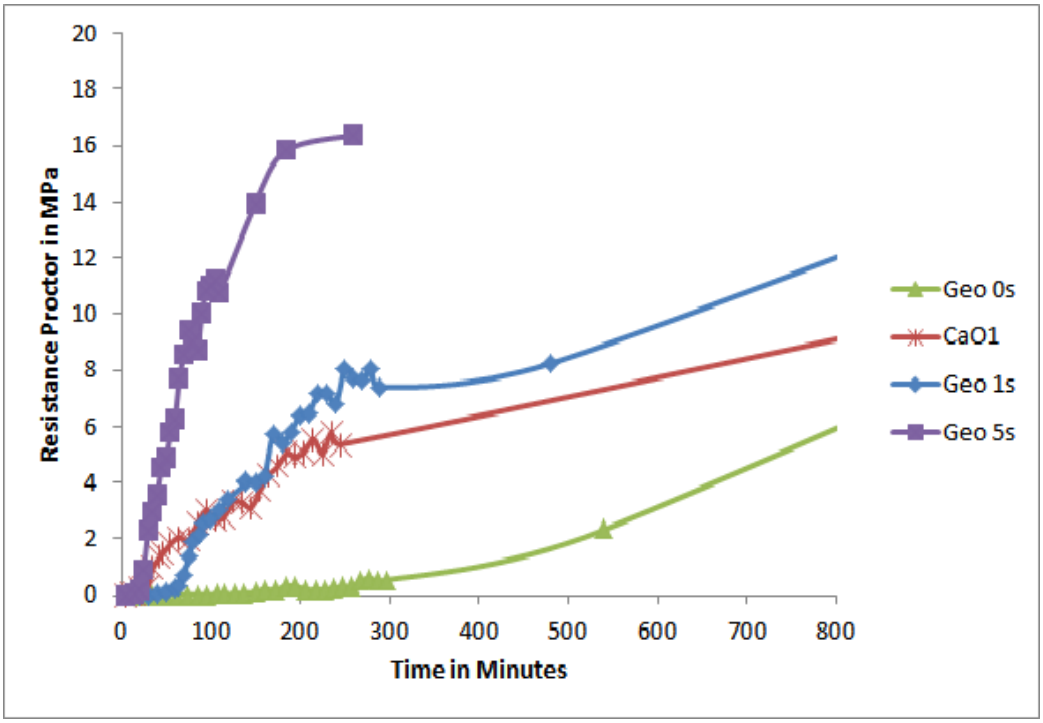

Figure 4.9: Proctor resistance of Geo 0s, CaO 1%, Geo 1s and Geo 5s

was added to flyash geopolymers instead of slag and the hardening rate was studied using UWR and Proctor penetration tests. Results were compared with mixes of equivalent slag content. Geopolymers made with CaO replacement equivalent to 5% (and more) were difficult to cast and compact in HIPS container as they hardened extremely rapidly. Therefore, CaO equivalent to 1% slag replacement was used for UWR measurements. Figure 4.8 and Figure 4.9 compares UWR measurements and proctor resistance of Geo 1s and CaO 1% respectively. Measurements of Geo 0s and Geo 5s are also included in both figures for reference. In Figure 4.8, the Geo 1s and CaO 1% curves overlap till 200 minutes, after which the rate of hardening for CaO 1% slows down. Whereas in Figure 4.9, the onset of proctor resistance is observed sooner in case of CaO 1% (20 minutes) compared to Geo 1s (80 minutes). The proctor resistance for CaO 1% increases rapidly till 200 minutes and slows down thereafter. However, in case of Geo 1s, the proctor resistance increases rapidly till 300 minutes after which it slows down.

It has been observed by Yip et al.[16] that the presence of calcium can significantly accelerate the hardening process. A similar observation was made by Llyod et al.[19] that the presence of calcium was critical to the early strength development in the geopolymer binders. It was proposed that early strength development was due to enhanced aluminosilicate geopolymer formation. This was either due to precipitated $Ca(OH)_2$ / calcium silicate hydrate providing nucleation sites or simply calcium acting as a charge balancer. However, the exact mechanism by which this takes place still remains unknown and requires further research. Since, slag is the only source of calcium in the mixes; a similar hardening mechanism can be expected.

Comparing the behavior of Geo 0s and CaO 1%(Figure 4.8), it is evident that the presence of calcium increases the rate of hardening of geopolymer mixes. When the behavior of Geo 1s and CaO 1% were compared, it was observed that curves overlap till 200 minutes after which the hardening rate of CaO 1% proceeds at slower rate than Geo 1s. The behavior was observed to be repeatable with variation between the runs less than 7%. Therefore, the hardening mechanism may be proposed as initiated by the precipitation of C-S-H and continued hardening is probably due to C-S-H acting as a site for nucleation. This is similar to the hypothesis proposed by Yip et al[16]. But the possibility of enhancement of geopolymer gel formation by calcium acting as a charge balancer cannot be excluded. The decrease in the rate

of hardening in the case of CaO 1% mix after 200 minutes may be because of decrease in the availability of free calcium ions in the system. After the initiation of hardening, as slag slowly releases calcium ions, hardening of Geo 1s continues for longer time compared to CaO 1%.

Proctor resistance of Geo 1s has a lag period of 60 minutes after which the Proctor resistance increases which matches with the rapid drop in s-wave reflection coefficient indicating strength development. The Proctor resistance of CaO 1% shows lag period of 20 minutes followed by rapid increase which slows down after 200 minutes indicated by change in the slope. Comparing the behavior of both the mixes, it is clear that the CaO 1% exhibits high initial Proctor resistance whereas Geo 1s shows higher Proctor resistance in the later ages.

In terms of strength development, strength gain is earlier with CaO 1% due to the instant availability of calcium ions forming C-S-H and rapidly increasing geopolymerisation by acting as a nucleation site. The strength development slows down with time as the availability of free calcium ions decreases. On the contrary, Geo 1s has low early strength and the hardening might have been initiated with the precipitation of C-S-H as calcium ions reached critical concentration. Initiation of hardening due to C-S-H could have been followed by rapid geopolymerisation as C-S-H acts as a nucleation site. Rapid geopolymerisation due to precipitation of C-S-H seems to be the reason for hardening in the both mixes for the initiation of hardening. But the hardening seems to slow down in the case of CaO1% after 200 minutes (UWR and Proctor) whereas it continues in the case of Geo 1s. Resistance offered by Geo 1s using proctor was always higher than the CaO 1% in the later ages. The strength development in the later ages is thought to be because of rapid geopolymerisation due to calcium acting as a charge balancer. This explains why Geo 1s continues to gain strength as slag releases calcium ions slowly compared to CaO 1% whose strength gain slows down due to the unavailability of free calcium ions. The hardening mechanism may be proposed as follows: after initiation of hardening by the precipitation of C-S-H, rate of geopolymer gel formation is increased as precipitated C-S-H provides nucleation sites. This might have been accompanied by aluminosilicate formation with calcium as charge balancer in the later stages of hardening. This hypothesis needs further investigation.

From Figure 4.7, only Geo 15s and Geo 10s have an extra peak within 50

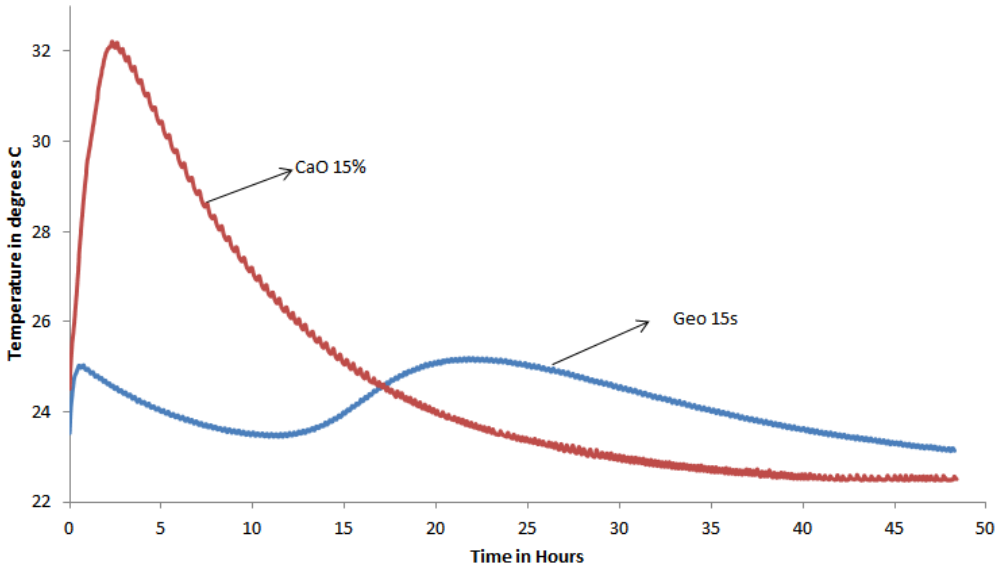

Figure 4.10: Semi-adiabatic calorimetry of CaO 15% and Geo 15s samples

hours and Geo 5s did not show any second peak within the experimental time frame. To compare the extent of chemical reaction between slag substituted geopolymer and CaO substituted geopolymer, Geo 15s and CaO 15%(Ca equivalent to 15% slag) were chosen. The semi-adiabatic calorimetry was conducted on them as shown in Figure 4.10. From Figure 4.10, CaO 15% mix shows a one large peak whose maximum temperature(32^0C) is much higher than that of Geo 15s(25^0C). Calorimetry curve of CaO 15% resembles that of cement paste with net temperature change of nearly 10^0 whereas the net temperature change in the case of Geo 15s is 2-3 ^{0}. The behavior of two mixes can be summarized as follows:

1. Geo 15s: After the initial wetting and initiation of hardening due to the formation of calcium silicate hydrate, reaction slows down due to unavailability of Ca ions given by the first peak. The reaction continues once the Ca ions have reached certain concentration where they could be acting as a charge balancers rapidly increasing geopolymerization given by the second peak

2. CaO: After the initial wetting and temperature rise due to CaO coming in contact with water (first few minutes), hardening is initiated due to rapid formation of calcium silicate hydrate. Chemical reaction slows

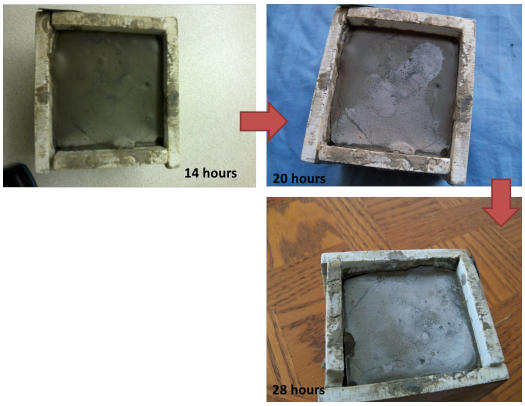

Figure 4.11: XRD pattern of Efflorescence, K: Aracanite

down as the calcium ions are no more freely available (rise and fall of one single peak).

Efflorescence was observed as early as 12 hours on the samples with high percentages of slag content and was also observed to increase with time (Figure 4.11). Efflorescence is thought to be one of the indications of insufficient geopolymerisation or excess alkali[25]. XRD and SEM-EDS were done on the efflorescent crystals to find out their composition and morphology. The white powder did not show any effervescence when added to HCl and XRD also did not indicate the presence of any calcium carbonate. In order to understand the nature of efflorescence, some fragments were scratched from the surface followed by analysis using SEM-EDS and XRD. Figure 4.12(a) gives the SEI micrograph of white powder seen on the surface. Figure 4.12(b) and Figure 4.13 respectively gives EDS analysis and XRD pattern of efflorescence confirming the presence of K_2SO_4. The carbon peak in the EDS spectrum is coming from the carbon tape and is not present in the crystals. The humps which are seen in the XRD pattern are because of the background holder.

Slag has 2.5% of sulfur by weight as seen from Table 3.1 and considering the fact that efflorescence is seen only in the mixes with high percentage of slag indicates dissolution of slag. Dissolution of slag implies the dissolution of calcium which is 37% by weight of slag (Table 3.1) as well. Since there was no indication of carbonation i.e. presence of calcium carbonate in efflorescence, it can be safely assumed that calcium was involved in the product formation eliminating the possibility of free calcium hydroxide in the system. Calcium hydroxide was not detected through XRD on the geopolymers

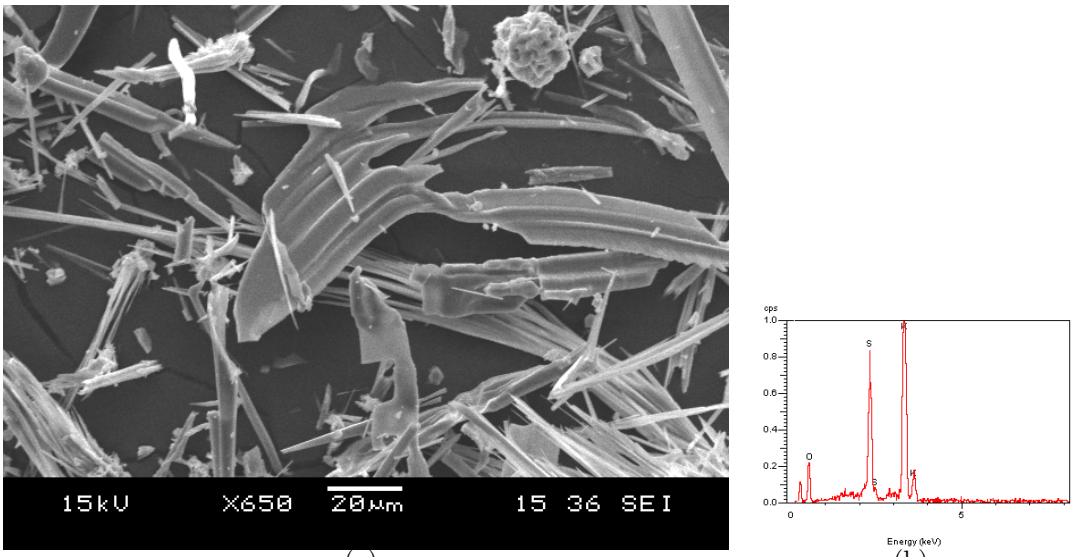

(a) (b)

Figure 4.12: a: SEM micrographs of Efflorescence seen on Geo10s and Geo15s, b: EDS on the crystals. K: Potassium, S: Sulphur, O: Oxygen

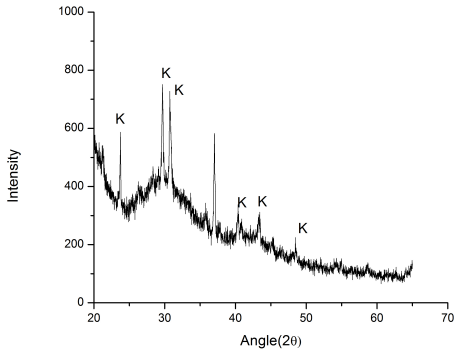

Figure 4.13: XRD pattern of Efflorescence, K:Aracanite

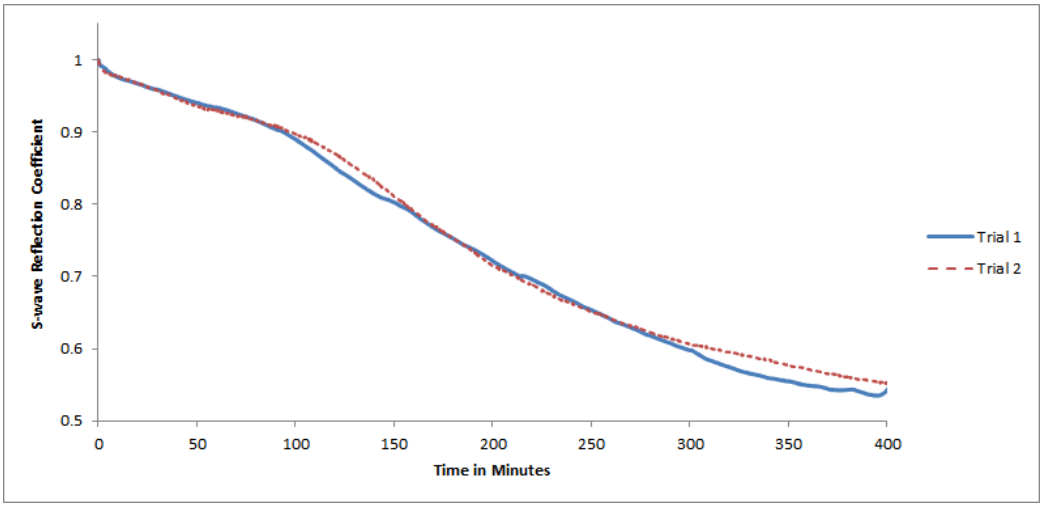

Figure 4.14: Reproducibility of UWR response is verified using CaO 1% mix

further confirming the observation.

4.6 Hardening Behavior of Different Mixes Using UWR

Reproducibility of s-wave UWR behavior of geopolymer mixes was tested by conducting three trials on the CaO 1% mix. The results are shown in Figure 4.14. The debonding times varied with the trials as seen previously with other systems because s-wave UWR is not sensitive enough for the debonding phenomenon. Therefore, the debonding behavior is curtailed in the Figure 4.14. The response from two different trials was overlapping indicating that the reproducibility is very strong. The other mixes were also repeated and the behavior was similar with variation between the mixes less than 7%. The validity of UWR method to monitor setting behavior of cement pastes and geopolymers was established by other studies and the present study, respectively. The behavior of geopolymer pastes by varying the amount of silicon was also studied in the present research. Two different SiO_2/K_2O ratios were investigated, SiO_2/K_2O = 1.94 and 1.25 and given in the Figure 4.15. Two different SiO_2/K_2O ratios (2 and 1.25) were also tested in the case of CaO 1% mix which is given in the Figure 4.16. The effect of SiO_2/Al_2O_3 ratios were investigated and reported elsewhere. From Figure 4.15, the onset of hardening for SiO_2/K_2O =1.94 and SiO_2/K_2O =1.25

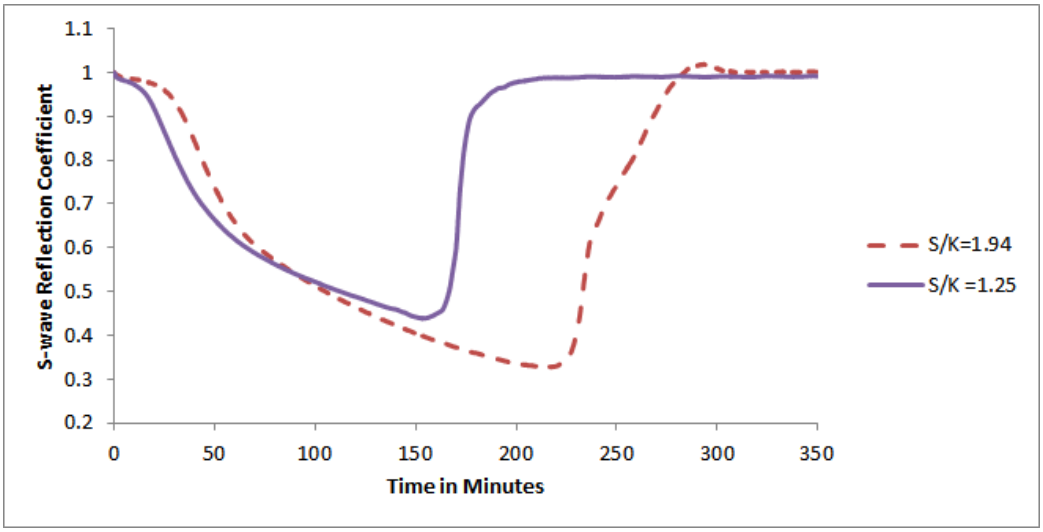

Figure 4.15: Effect of extra silicon on the hardening rate of flyash-slag geopolymer monitored using UWR. S/K = SiO_2/K_2O

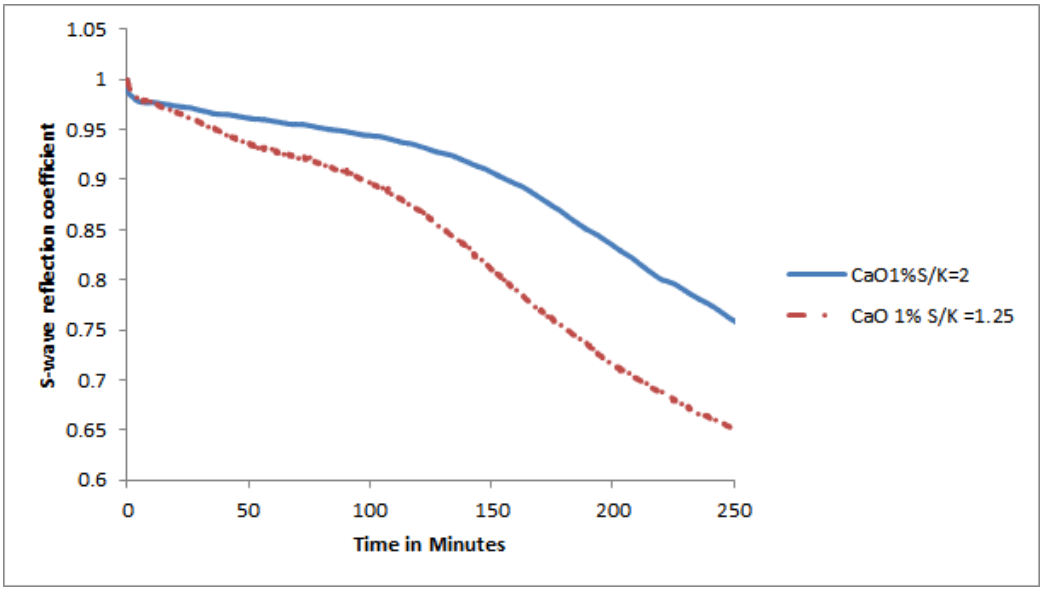

Figure 4.16: Effect of extra silicon on the hardening rate of flyash-CaO geopolymer monitored using UWR. S/K = SiO_2/K_2O

are 25 minutes and 10 minutes, respectively. From Figure 4.16, the onset of hardening for SiO_2/K_2O =1.94 and SiO_2/K_2O =1.25 are 135 minutes and 85 minutes respectively. The similar behavior was observed by different authors that the setting is delayed with the addition of excess silicon in the system[27]. The reason for the delayed onset of hardening was attributed to the presence of extra Si in the system. Increasing amount of silicate species is available for condensation and reaction between silicate species with the increasing Si content in the system. This makes the system dominant in oligomeric silicates. Since the rate of condensation between silicate species is slower than that between aluminate and silicate species, setting occurs later with increasing Si content. This delayed setting was clearly observed using UWR which further strengthens the validity of the method to study unconventional systems like geopolymers.

4.7 Conclusions

The following conclusions were drawn from UWR and proctor studies of geopolymer solids:

1. Onset of hardening depends on the percentage of slag in the flyash-slag geopolymer. Higher the slag percentage, earlier the hardening begins.

2. S-wave ultrasonic wave reflection method results correlate well with proctor penetration tests in terms of predicting hardening behavior.

3. UWR behavior for geopolymer pastes showed good reproducibility with a variation between mixes close to 7%.

4. Debonding behavior was predicted better by P-wave UWR compared to s-wave UWR because P-wave are more sensitive to air gap than s-waves.

5. Calorimetric response showed higher chemical reaction in the presence of high slag contents.

6. Calcium coming from slag is suspected to be the reason for high hardening rate. The possible hypothesis was proposed as follows: after the

initiation of hardening due to the precipitation of C-S-H, further hardening is caused due to the rapid geopolymerisation with Ca ion acting as a charge balancer.

7. Efflorescence was due to precipitation of potassium sulfate and not calcium carbonate indicating the absence of free calcium ions. This further supports the theory that calcium is involved in the product formation.

8. UWR has successfully predicted the effect of extra silicon on the setting behavior of geopolymer mixes.

9. UWR will be a useful tool for predicting the setting behavior of non-conventional concrete systems like geopolymers.

Chapter 5

Characterization of Solid Geopolymer Product

As discussed earlier in chapter 4, onset of hardening may be associated with the initial formation of calcium silicate hydrate followed by the rapid geopolymerisation. This hypothesis needs further proof and this chapter makes an attempt towards characterizing the geopolymer solids and relate with hardening. Conventional techniques like scanning electron microscopy (SEM) and x-ray diffraction (XRD) methods were used but were found to be inadequate which will be discussed in this present chapter. Since, classical powder XRD technique fails at characterizing amorphous compounds like geopolymers, fourier transform infrared spectroscopy (FT-IR) was adopted for the study. The primary interest of this chapter was to study changes responsible for the onset of hardening as predicted by UWR. However, attention should be drawn to the fact that the presence of Si-O-T (T =Al, Si) vibrations of different origins, namely from the initial ash, geopolymer product and calcium silicate hydrate, yields an overlapping spectrum band resulting in a broad hump whose correct interpretation is rendered difficult.
In order to overcome this difficulty, the activated flyash was subjected to various chemical attacks which are described in the chapter 3. The salicylic acid-methanol (SAM) extraction separates calcium silicates from the initial ash and geopolymer. Whereas the HCl treatment differentiated the initial unreacted ash from the amorphous geopolymer products and calcium silicates.

5.1 X-ray Diffraction

X-ray diffraction was done on samples collected at various ages which were chosen based on the UWR and calorimetric responses. For example, one of the samples was collected at the age corresponding to onset of hardening

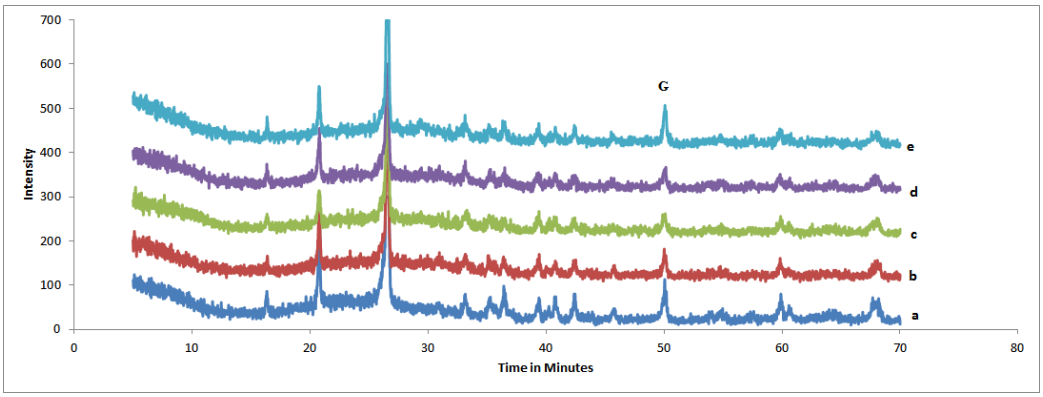

Figure 5.1: a: Flyash+15% slag, b: Geo 15s 60 minutes, c: Geo 15s 10 hours, d: Geo 15s 24 hours, e: Geo 15s 14 days. G: Gismondine, other peaks are named in Figure 3.5. XRD patterns of Geo 15s at various ages' shows that there was no difference in the patterns with age other than decrease in the intensity of certain Quartz and Mullite peaks. The appearance of Gismondine was indicated by the increase in intensity of $50^0 2\theta$ at an age of 14 days

from UWR and the others depending on the peak positions from calorimetric curve. The geopolymer samples collected at various ages were compared with the base, flyash+slag (raw material). The XRD patterns of geopolymers samples collected at early ages did not differ to any great extent from that of initial raw material, in fact they overlapped perfectly. Having known from the calorimetric curves and UWR curves that Geo 10s and Geo 15s have higher strength development and greater amount of reaction, Geo 15s was chosen to study the changes in phases using XRD.

Figure 5.1 gives XRD patterns for raw material and Geo 15s at an age of 60 minutes, 10 hours, 24 hours and 14 days. The Geo 15s sample of age 60 minutes did not differ from the XRD pattern of flyash+slag sample and a similar observation was made with the sample which was 10 hours old. It was observed that the XRD pattern of geopolymer which was 24 hours old showed a 1/2 degree shift to higher 2θ angle compared to that of original raw material. This indicates the formation of a product with low range order. The shift was accompanied by decrease in the intensity of certain peaks. Therefore, this shift might have happened slowly with time. The sample at 14 days showed increase in intensity of 50^0 2θ.

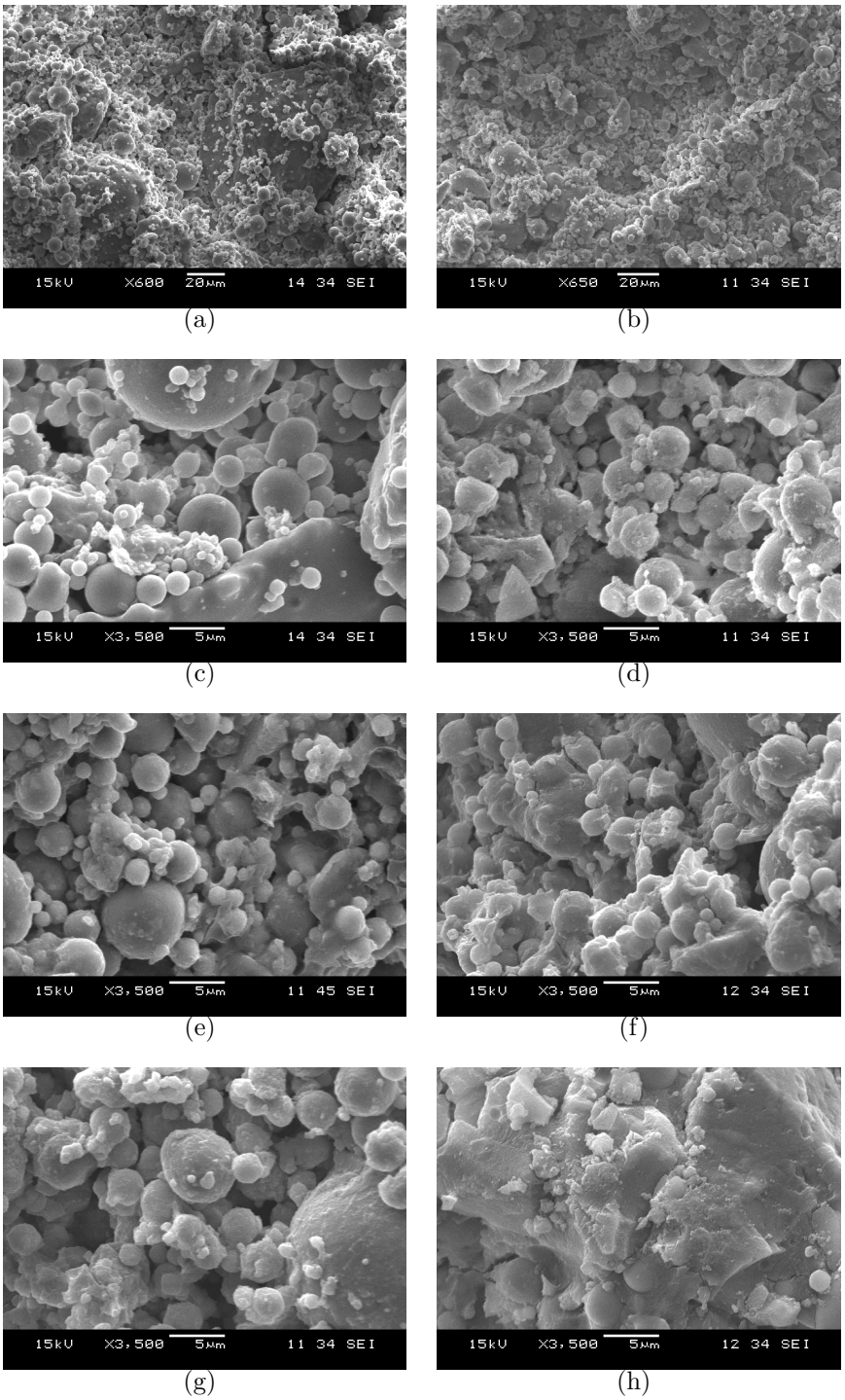

Figure 5.2: a and c: Geo 0s-3 hours, b and d: Geo 15s-3 hours, e: Geo 0s-24 hours, f: Geo 15s-24 hours, g: Geo 0s-14 day, h: Geo 15s-14 day

5.2 Scanning Electron Microscopy

Geo 0s and Geo 15s were chosen to study the effect of slag on microstructure using SEM. These two mixes were chosen because they represent the extreme

case of microstructural development. Figure 5.2 shows an SEM micrograph of flyash based geopolymer with and without slag replacement (Geo 15s and Geo 0s). Figure 5.2(a) and Figure 5.2(c) gives the micrograph of Geo 0s at an age of 3 hours at two different magnifications. Figure 5.2(b) and Figure 5.2(d) gives micrographs of Geo 15s at an age of 3 hours at two different magnifications. At lower magnification, the distinction between microstructures of Geo 0s and Geo 15s was not very clear. The product formation was seen in the case of Geo 15s whereas Geo 0s sample does not show as much product formation. In the case of Geo 0s, at higher magnification (Figure 5.2(c)) it was apparent that there had been no dissolution of the flyash spheres. The microstructure can be described as a dense network of flyash spheres held together by no interconnectivity. This was also confirmed from the calorimetry and UWR responses indicated by a very slow reaction. On the other hand, in the case of Geo 15s (Figure 5.2(d)), the formation of product is evident on the surfaces of flyash. The particle morphology of flyash spheres did not change markedly but they are connected by gel like network. The presence of slag caused more product formation resulting in the gel network increasing the interconnectivity. The difference in microstructures further explains the reason for the high hardening rate of Geo 15s compared to Geo 0s. A significant degree of porosity is seen in the microstructure at this age. These observations are consistent with other studies.[5]

At higher magnification, the difference between the microstructure of Geo 0s and Geo 15s of age 24 hours is rather clearer. The porosity is seen to decrease with time in the case of Geo 15s which is not seen any more by the age of 14 days. The gel like network similar to the samples at the age of 3 hours was seen in the samples which are 24 hours old, connecting the flyash spheres. At an age of 14 days, flyash spheres are densely covered with gel and no clear distinction can be seen. There seems to be significant porosity in the case of Geo 0s even at the age of 14 days as product is seen only to form on the surface of flyash spheres with minimum interconnectivity. Davidovits et. al[5] has proposed that the geopolymerisation without thermal activation can be regarded as a superficial reaction based on diffusion mechanism and not a complete dissolution and precipitation process. Microstructure seen at early ages can be described based on above theory. Appearance of new peaks was not observed indicating that there were no new crystalline products formed however the sample of age 14 days has indicated the presence of

Gismondine ($CaAl_2Si_2O_8, 4H_2O$), an aluminosilicate zeolite mineral. Since the main peaks of Gismondine coincided with that of quartz, the Gismondine peaks were concealed. Therefore, the possibility of Gismondine forming in the early age cannot be ruled out. The increase in peak intensity at $50^0 2\theta$ was attributed to the formation of Gismondine. This also supports the observation that calcium is involved in the formation of aluminosilicate geopolymer. The appearance of this peak indicates ongoing reaction with time, which is also supported from increase in compressive strength with age as seen from Table 4.1.

5.3 Effect of Acetone Treatment

Acetone was used to stop the reaction at designated times to prepare samples for characterization. The effectiveness of acetone to stop the reaction was tested by comparing the XRD patterns of samples treated with acetone with those samples that were not treated. The following was the methodology adopted and the XRD patterns are given in the Figure 5.3:

1. Run XRD on the sample which was 24 hours old and treated with acetone (24hA+24XRD)

2. Run XRD on the sample that was stored in the vacuum for 20 days and treated with acetone at the age of 24 hours (24hA+20dXRD)

3. Run XRD on the sample which was 20 days old and treated with acetone at the age of 20 days (20dA+20dXRD)

From Figure 5.3, the XRD patterns of 24hA+24hXRD, 24hA+20dXRD and 20dA+20dXRD are similar and no new peaks are observed indicating that either the acetone was not effective in stopping the reaction or that the reaction has stopped after 24 hours. However, the SEM investigation has revealed that the microstructural development continued with time. The microstructure at 14 days (Figure 5.2(h)) seemed more dense compared to the microstructure at 24 hours(Figure 5.2(f)) indicating the ongoing development of microstructure. This was also established by the increase in compressive strength with age (Table 5.1). Micrographs clearly distinguish the samples that were 24 hours old and 14 days old which also explain the compressive

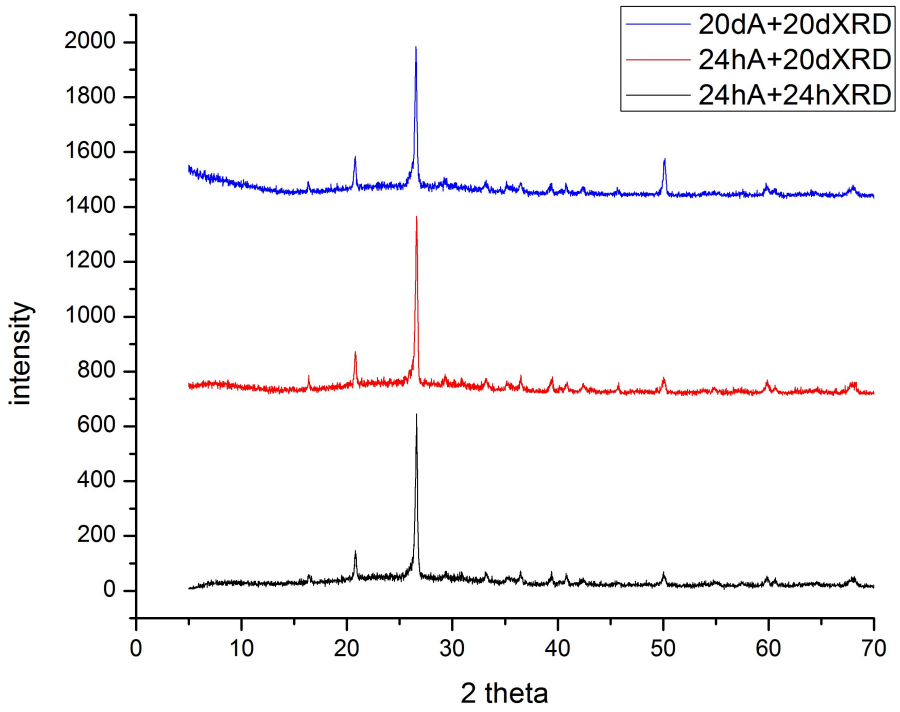

Figure 5.3: XRD patterns of samples tested for determining effectiveness of acetone in stopping the reaction

strength results. Therefore, the reason that reaction has stopped after 24 hours does not explain the XRD results. Thus, the effectiveness of acetone in stopping the geopolymer reaction cannot be concluded from the XRD patterns. The technique that is more sensitive to changes in amorphous product like FT-IR should be used. FT-IR and XRD methods were used simultaneously to characterize geopolymer solids. Based on UWR and semi-adiabatic calorimetric curves, time periods of 10 minutes, 60 minutes, 10 hours, 24 hours and 14 days were chosen to characterize geopolymer solid for Geo 15s sample. FT-IR and XRD were also conducted on solid residues after SAM and HCl extraction methods. Relevant spectral subtractions were performed to maximize the volume of information that can be obtained from the data. Semi adiabatic calorimetry was also performed to substantiate the information. Geo 15s was chosen for these studies because it is known from the other experiments to show maximum microstructural development. To prove the hypothesis proposed in chapter 4, CaO equivalent to 15% slag was added to flyash and above mentioned experiments were conducted. The amount of calcium that was coming from slag was compensated by the addition of CaO. Silicon and aluminum were compensated by adding extra flyash and extra potassium silicate. Water to solids ratio was kept constant for all the mixes.

Table 5.1: 3, 7 and 14 day compressive strength of Geo 15s (average of three cylinders)

Days	Compressive strength in MPa
3	19.2
7	21.2
14	33

5.4 Flyash-slag Geopolymer

Mix design as described in the chapter 3 was followed for preparing Geo 15s. Powdered samples for FT-IR and XRD at 10 minutes, 1 hour, 10 hours, 24 hours and 14 days were collected by treating the crushed solid with acetone. This powdered sample was stored in the vacuum desiccator until testing. SAM extraction and HCl extraction were done on these powdered samples

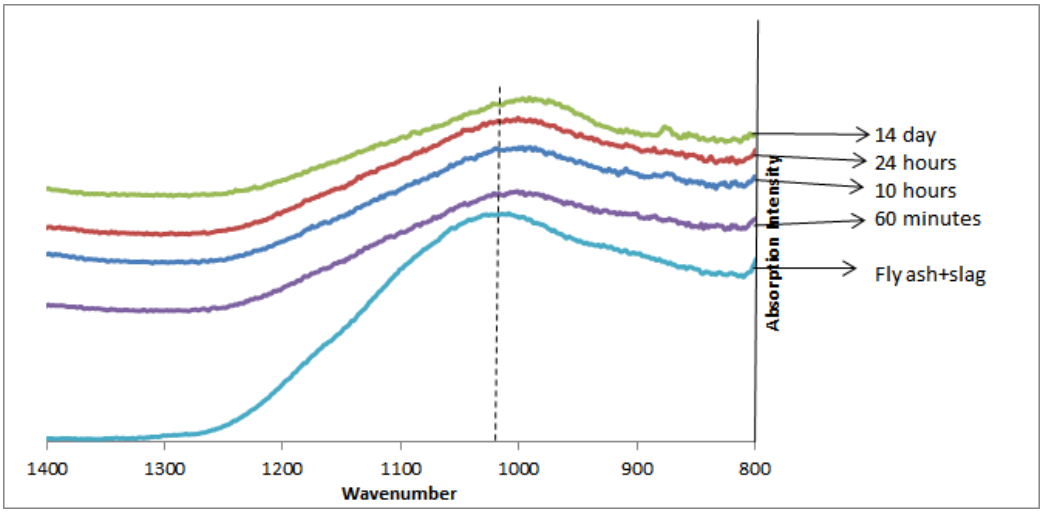

Figure 5.4: FT-IR spectrum of Geo 15s samples with time. Shift in the main peak towards lower wave numbers is observed. Absorption intensity on Y-axis and all curves are offset

as described earlier in chapter 3. FT-IR spectra are given either in transmission mode or absorption mode depending on the clarity of the spectrum. Spectra were analyzed for main asymmetric stretching vibration of Si-O-T which lies between 1100-900 cm^{-1}. The Si-O-T asymmetric stretching vibration band will be referred to as the main band. FT-IR spectra of Geo 15s with time was given in the Figure 5.4. The spectrum for pure flyash and pure slag are taken separately and added in the ratio to obtain the spectrum for raw material. In the Figure 5.4, the main Si-O-T asymmetric band in the case of raw material(flyash+slag) was marked at 1028 cm^{-1}. The vibration spectra of vitreous or amorphous materials unlike crystalline materials have very broad rather imprecisely defined bands which makes interpretation difficult. This is also seen in the figure. If there was mid-range order in the glass structure, the bands corresponding to the tetrahedral structural unit vibrations would appear in mid-IR spectra of silica glasses. There is also an acknowledged resemblance in mid-range order for amorphous and crystalline silicates[28].

In the Figure 5.4, the band associated with Si-O-T asymmetric stretching vibration shifts perceptibly to a lower frequency with time. The exact position of this band depends on the Al/Si ratio of the product and also to be determined by the Al atom content per unit of formula[21]. The band shifts to lower frequencies as the Al substitution increases. Si-O-T angle reduces

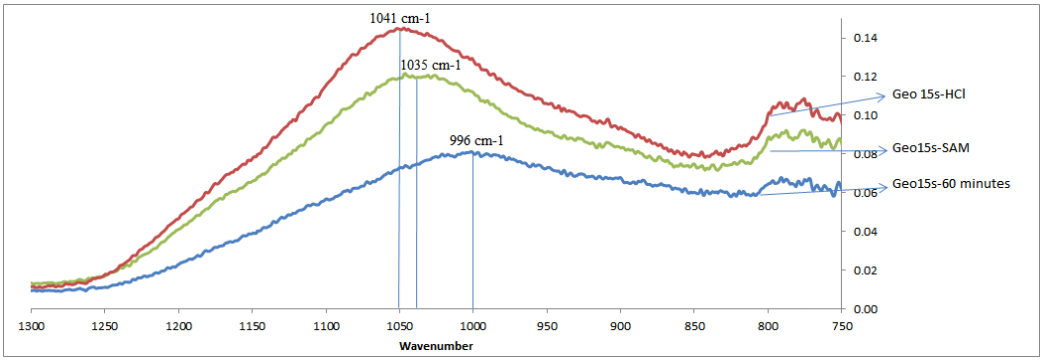

Figure 5.5: FT-IR spectrum of 1 hour old Geo 15s sample. IR spectrum of insoluble residue from SAM treatment and HCl treatment are also given. Absorption intensity is on the Y-axis and various spectra are offset

when Al^{3+} substitutes Si^{4+} and the bond force constant of Si-O-Al bond is smaller than that of Si-O-Al bond. Due to these reasons, signal appears at a lower frequency with Al substitution. Figure 5.1 gives XRD patterns of Geo 15s at 60 minutes, 10 hours, 24 hours and 14 days along with the raw material. As described earlier in the XRD section, XRD does not detect the changes happening with time. Only the sample at 14 days shows one new peak. To clearly look at this new peak, a few important samples like the one at 14 days was run for XRD at a rate of 0.15 degrees per minute between 27^0 to 35^0 2θ.

5.4.1 Sample at 60 minutes

Figure 5.1 shows that XRD pattern of Geo 15s at 60 minutes has not differed much from its base raw material. However, Figure 5.4 shows that the main asymmetric band has shifted to a lower frequency within 60 minutes. Therefore, further studies were done on the sample at 60 minutes as given in the Figure 5.5. The sample was also treated with SAM and HCl to analyze the products formed. Figure 5.5 gives that Geo 15s at 60 minutes has main band with peak centered at 996 cm^{-1} and after SAM extraction the band moved back to 1035 cm^{-1}. This indicates that some products have been dissolved in SAM indicating the presence of calcium silicates. SAM does not dissolve slag and therefore the shift would have been only due to dissolution of calcium silicates formed. After HCl treatment, the band moves to 1046 cm^{-1} which was nothing but unreacted flyash+slag. Apparently, HCl treatment did not

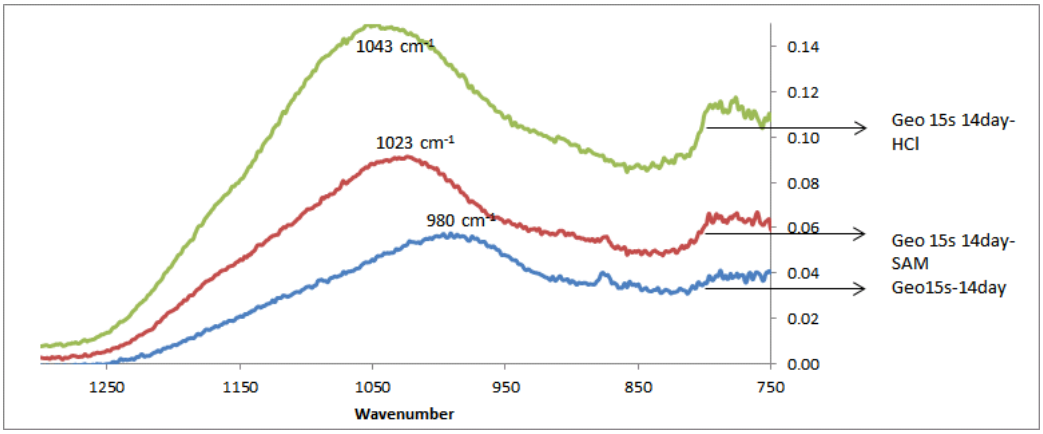

Figure 5.6: FT-IR spectrum of 14 day old Geo 15s sample and IR spectrum of insoluble residue from SAM and HCl treatments. Absorption intensity is given on Y-axis

dissolve unreacted slag however, the effect of HCl on slag should be further studied.

5.4.2 Sample at 14 days

IR spectrum of Geo 15s at an age of 10 hours and 24 hours also show a similar shift as seen from the Figure 5.4. From Figure 5.1, Geo 15s sample at 14 days shows one new peak. Therefore, the sample at 14 days was analyzed for IR. XRD on 14 day sample which was run from 27 degrees 2θ to 35 degrees 2θ is also given. IR and XRD were done on insoluble residues obtained after SAM extraction and HCl extraction as well. Figure 5.6 gives that Geo 15s at 14 days has a main band with peak centered at 980 cm^{-1} and after SAM extraction the band moved back to 1023 cm^{-1}. After the HCl treatment, the band moves to 1043 cm^{-1} which was same as the band for unreacted flyash(Figure 3.6). This further confirms that the HCl treatment has been dissolving the geopolymer products leaving behind the unreacted flyash. However, the main band of initial raw material (flyash+slag) was at 1028 cm^{-1}(Figure 5.4). The initial raw material was a combination of flyash and slag and as the slag was consumed in the reaction much faster than the flyash; the unreacted raw material would just be flyash. The amount of insoluble residue after SAM treatment was calculated per 1 gram of initial material and was found out to be 0.48 grams indicating that 0.52 grams was

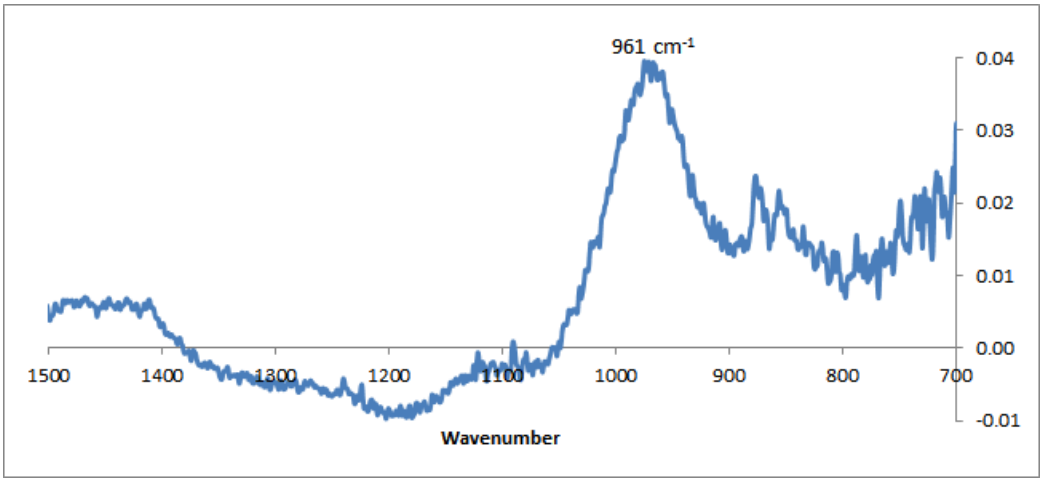

Figure 5.7: FT-IR spectrum of C-S-H obtained after subtracting the spectrum of 14 day old Geo 15s sample with the IR spectrum of insoluble residue from SAM extraction

dissolved in SAM. The spectra were subtracted in a percentage proportional to this calculated amount and given in the Figure 5.7. It shows that there was single peak at 960 cm^{-1} which represents C-S-H as mentioned in the literature[29]. This confirms the presence of C-S-H. Spectrum also indicates some region in the negative axis and this could be because of inappropriate weight calculations. This could be avoided by measuring the weight more carefully. This calculation was not performed on samples after HCl treatment due to errors in weight measurements caused by following reasons:

1. Iron lost due to magnet used for stirring salicylic acid-methanol and HCl
2. Some fines lost while vacuum filtration
3. After HCl treatment and subsequent filtration, insoluble residue should be calcined at 1000^0C which was avoided previously.

The problem due to iron loss can be avoided by either using the ultrasonic bath to stir the samples or remove iron before the treatment. This could also be alleviated by using a physical rotor for stirring. Loss due to vacuum filtration can be avoided using a better filtration paper. These problems will be resolved and taken care in future experiments. The broad hump centered around 29.4 degrees 2θ disappears leaving a peak at 29.4 degrees 2θ from

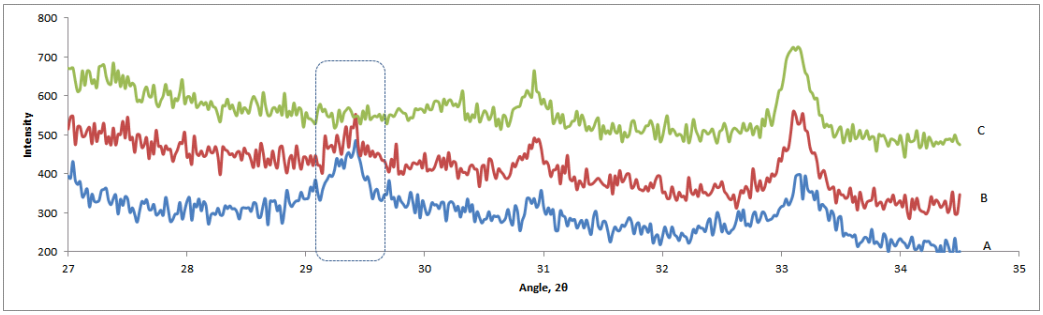

Figure 5.8: A: XRD pattern of Geo 15s at 14 days, B: XRD pattern of insoluble residue after SAM treatment, C: XRD pattern of insoluble residue after HCl treatment, Marked rectangle represents disappearance of peak at 29^0 2θ

the XRD pattern of insoluble residue after SAM extraction (Figure 5.8). This indicates that calcium silicates have dissolved further confirming their presence. The peak at 29.4 degrees 2θ disappears completely after HCl treatment (Figure 5.8). This could be because of the presence of $CaCO_3$ or some geopolymer solid.

5.5 CaO Equivalent Mixes

Effect of calcium on the hardening of flyash geopolymers was conducted by substituting CaO for equivalent amount of slag as described earlier in the chapter 4. Since, Geo 15s was chosen for the study, CaO equivalent to 15% slag was used in the present chapter. This was represented as CaO 15%. Samples of two different ages namely 1 hour and 24 hours were chosen to compare with equivalent Geo 15s. XRD and FT-IR were done on both the samples. Figure 5.9 and Figure 5.10 give XRD patterns of CaO 15% sample of age 1 hour and 24 hours respectively. Figure 5.11 gives FT-IR done on both the samples including the spectrum of the insoluble residues after SAM treatment and HCl treatment.

From Figure 5.9, three main peaks of CaO (37.5, 54.0 and 32.3 degrees 2θ) appear in the CaO 15% sample which was 1 hour old indicating the presence of unreacted CaO. Peak at 29.4^0 2θ which was seen in the original sample seem to disappear after the SAM extraction along with CaO peaks. This peak can be associated with $CaCO_3$ or the presence of calcium silicate hy-

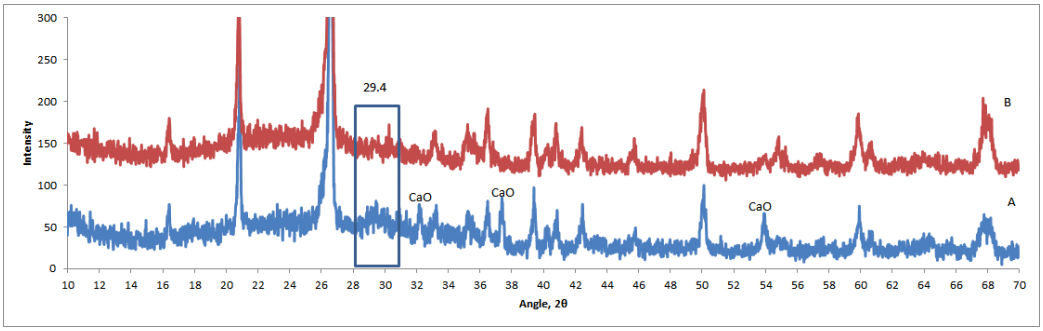

Figure 5.9: A: XRD pattern of 1 hour old CaO 15% , B: XRD pattern of insoluble residue after SAM treatment. Marked rectangle represents disappearance of peak at 29 degrees 2θ. Three main peaks of CaO are represented and CaO which disappeared after SAM extraction.(PDF:75-0264)

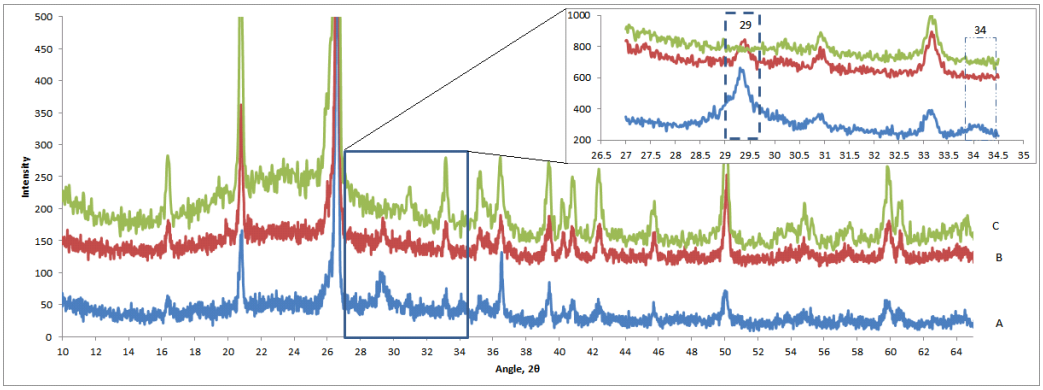

Figure 5.10: A: XRD pattern of 24 hours old CaO 15%, B: XRD pattern of insoluble residue after SAM treatment, C: XRD pattern of insoluble residue after HCl treatment, Marked rectangle represents close up view of A, B, C from 27^0 2θ to 35^0 2θ

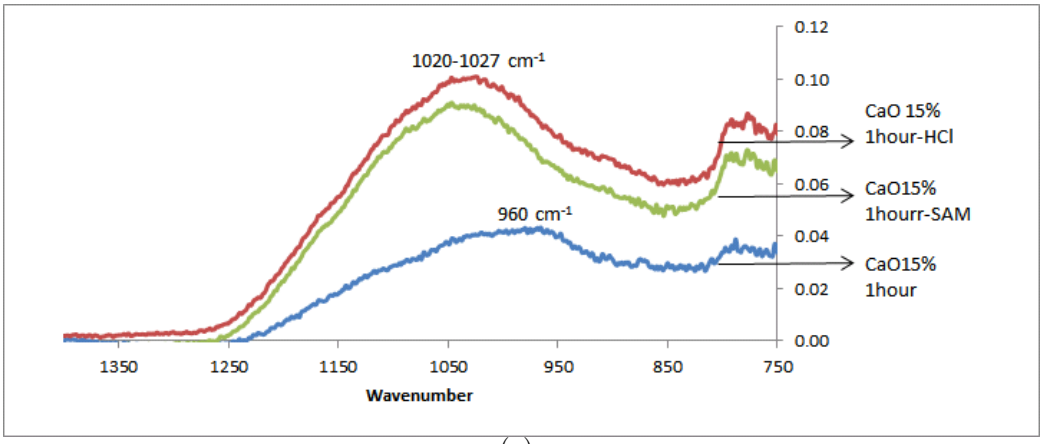

(a)

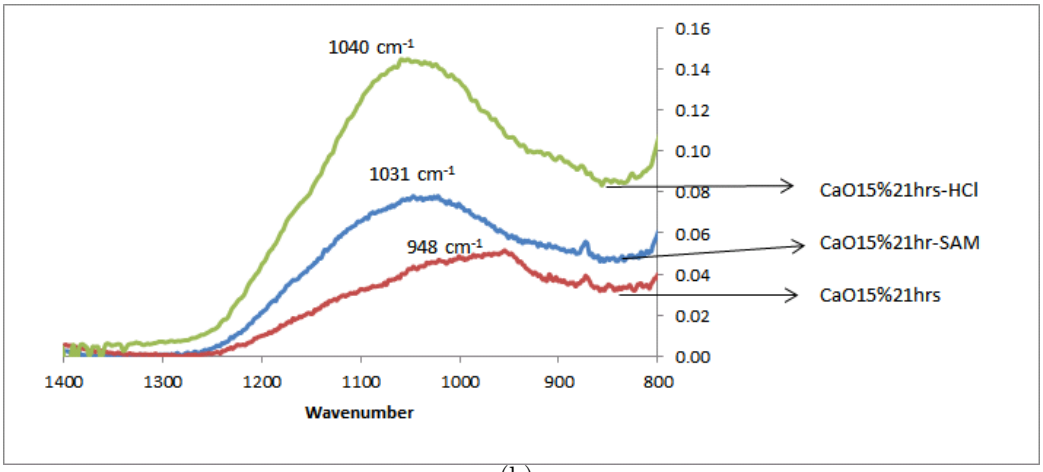

(b)

Figure 5.11: a: IR spectrum of CaO 15% 1 hour sample, Insoluble residue after SAM extraction and after HCl extraction, b: IR spectrum of CaO 15% 24 hours sample, Insoluble residue after SAM extraction and after HCl extraction

drate. Since $CaCO_3$ does not dissolve in SAM, it is more positively associated with the presence of calcium silicates. This indicates that calcium silicate hydrate was formed in the early ages. Geo 15s at 1 hour also shows some C-S-H which was evident not through XRD but only through FT-IR. This illustrates that C-S-H formed in the presence of CaO was more crystalline compared to C-S-H formed in the presence of slag. This might be due to the free availability of calcium resulting in higher Ca/Si ratio thus leading to the crystalline C-S-H.

After SAM treatment, the main band in the IR spectrum of the insoluble residue moved to a higher frequency, from 960 cm^{-1} to 1020-1027 cm^{-1}(Figure 5.11(a)). After HCl treatment, the shift in the IR spectrum of the insoluble residue was also 1020-1027 cm^{-1}. Hence, the only product formed in the early age could be calcium silicate. It should be taken note that the frequency of main band in the insoluble residue after HCl treatment does not match with the frequency of main band of raw material from Figure 5.4. This is because the raw material was flyash+slag but here it is rather flyash+CaO. Therefore, the shift should not be compared with flyash+slag. XRD reveals the presence of unreacted CaO which would react with HCl to form calcium chloride along with carbon-dioxide and water. Therefore, spectrum of insoluble residue after HCl treatment could be due to the combination of unreacted fly ash and leftover calcium chloride. This reasoning could be validated by stating that calcium chloride has a peak at $\tilde{1}000$ cm^{-1}[30]. The final position of the main band would be determined by an overlap of the band from flyash and from calcium chloride and therefore the peak position in the Figure 5.11(a) was not the same as that of unreacted flyash. To overcome this difficulty and to be able to compare with the original fly ash, insoluble residue should be calcined at 1000^0C to eliminate such products and to remove extra water resulting from the reaction.

In the case of 24 hour old CaO 15%(Figure 5.10), absence of CaO peaks indicate that most of CaO has reacted. A broad hump is seen at 29.4^0 2θ which represents the presence of an amorphous product. The broad hump disappears and a peak appears at the 29.4^0 2θ which further disappears after HCl treatment. The broad hump at 29.4^0 2θ might represent the presence of calcium silicate which disappears after dissolving in SAM. The peak at 29.4^0 2θ that is seen in the insoluble residue after SAM extraction could be some crystalline zeolite or geopolymer since it disappears after HCl treat-

ment. The main band in Figure 5.11(b) shifts to a lower frequency, 948 cm^{-1} after 24 hours of reaction time compared to 960 cm^{-1} at 1 hour indicating that the Al substitution has been taking place. The position of main band is different in both insoluble residue after SAM extraction (1030 cm^{-1}) and insoluble residue after HCl extraction(1041 cm^{-1}). The frequency of main band after HCl treatment is similar to the frequency of main band in fly ash(Figure 3.6). This is different from the frequency of main band seen in insoluble residue of CaO 15% 1 hour sample after HCl treatment. This is because CaO was completely consumed by 24 hours as revealed by XRD and CaO was not left behind to react with HCl.

The amount of insoluble residue after SAM treatment was calculated per 1 gram of initial material and was found out to be 0.46 grams indicating that 0.53 grams was dissolved in SAM. The spectra were subtracted in a percentage proportional to this calculated amount and given in the Figure 5.12. It shows that there is single peak at 950 cm^{-1} which represents C-S-H as mentioned in the literature[29]. This confirms the presence of C-S-H. Spectrum also indicates some region in the negative axis and this could be because of inappropriate weight calculations. This could be avoided by measuring the weight more carefully. This peak matches with that obtained with Geo 15s 14 day sample which further validates the presence of C-S-H. Comparing Geo 15s and CaO 15%, the presence of calcium silicate was detected in the early ages. Geopolymer solids along with calcium silicate hydrate were found in the later ages. This further supports the theory that the hardening would be initiated with the precipitation of calcium silicate hydrate followed by geopolymerisation. This was explained by the presence of both geopolymer and calcium silicate hydrate at later ages. One large peak observed in the calorimetric curve for CaO 15%(Figure 4.10) represents the rapid formation of C-S-H which is also proved from XRD and FT-IR.

5.6 Characterization of Pore Solution

Characterization of geopolymers remains a challenge because of their amorphous nature. The main aim of the present chapter was to determine the role of calcium in the hardening of flyash geopolymers. It is also important to study interaction between calcium, silicon and aluminum. It is not possible

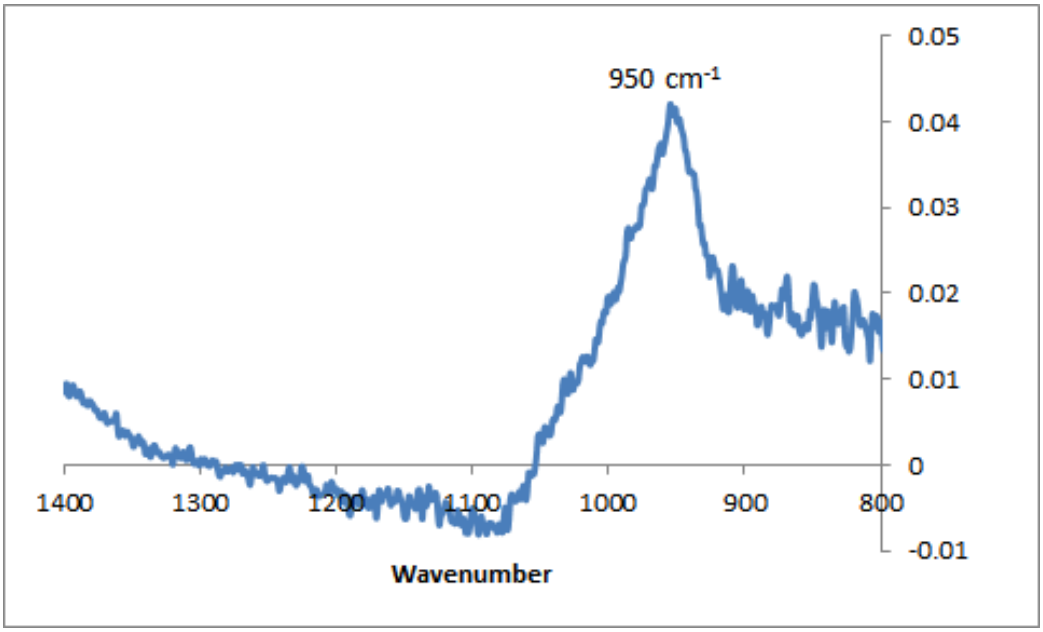

Figure 5.12: FT-IR spectrum of C-S-H obtained after subtracting the spectrum of 24 hours old CaO 15% sample with IR spectrum of insoluble residue from SAM extraction

to study the interaction at the level of ionic species using any of the methods described previously. There is very little information available in the literature about the chemistry of pore solution in geopolymers at early ages, whereas the pore solution chemistry of ordinary Portland cement hydration is fairly well documented. More information about the hardening process can be sought by studying the variation in ion concentration with time and relate it with the solid characterized using XRD and FT-IR. Therefore, pore solution was extracted and studied. The extraction of pore solution and analysis was done as discussed in chapter 3. Extraction and analysis using ICP-MS was done at least three times. However, error between trials was observed to be very high. The reasons could have been following:

1. Sample getting contaminated due to the presence of DI water in the syringe barrel after cleaning thus diluting the concentration

2. Giving wrong theoretical estimations for ion concentrations

The process of pore solution extraction needs to be studied in detail with conventional mixes like cement pastes to solve the above mentioned problems before using it for geopolymers. From the literature, pore solution for cement

pastes were extracted using Dye method as described by Diamond et al.[31]. There were several improvements of this method[32]. Attempts are being made presently to extract pore solution using this dye method. One study by Provis et al. on pore solution of geopolymers was conducted using the Dye method[33]. However, the study mainly concentrates on long term properties unlike the interest of the present study.

5.7 Conclusions

The following conclusions were drawn from the present chapter on solid characterization:

1. X-ray diffraction along with FT-IR can give valuable information about the geopolymer solids

2. SEM micrographs explain the difference in the hardening behavior of with and without slag substituted flyash geopolymers

3. XRD and FT-IR studies conducted on slag substituted geopolymers and CaO substituted geopolymers have given indication of presence of calcium silicate hydrate in the early stages of reaction. This supports the hypothesis that initiation of hardening was due to the precipitation of calcium silicate hydrate

4. XRD and FT-IR studies conducted on later age samples proved the presence of geopolymer solids and highly Al substituted C-S-H

5. The amount of Ca ion available determines the nature of solids formed

Chapter 6

Summary and Key Conclusions

The main objective of present research was to study the early age properties of flyash-slag geopolymer and explore the microstructural and chemical changes responsible for the hardening. The other aim was to understand the role of calcium to optimize properties of user-friendly geopolymer. S-wave UWR and proctor penetration methods were used for the first time in this study to continuously monitor the hardening process of fly ash-slag geopolymers. Microstructural development was monitored using SEM. XRD and FTIR were used in conjunction to characterize geopolymer product and pore solution was analyzed for concentration variation of ions like silicon, calcium and aluminum with time.

As the percentage of slag was increased, workability decreased and compressive strength increased. It was a tradeoff between the early age and later age properties. UWR and proctor have revealed that as the amount of slag increased, not only did workability decreased but also the time for onset of hardening. UWR and proctor results correlated very well. Initial and final setting times were not defined for geopolymer having not able to define the meaning in terms of microstructural changes. UWR has succesfully predicted the effect of extra silicon on the behavior of geopolymer pastes. UWR along with proctor penetration method can be a useful technique for monitoring setting of geopolymers. Fly ash-slag geopolymers can be characterized under rapid stiffening mixes.

UWR and proctor penetration tests conducted on various slag substituted and CaO substituted geopolymers has given an important information about the hardening behavior. The hardening mechanism was proposed as follows: after initiation of hardening by the precipitation of CSH, rate of geopolymer gel formation is increased as precipitated CSH provides nucleation sites. This might have been accompanied by aluminosilicate formation with calcium as charge balancer in the later stages of hardening. This hypothesis

needs further proof. Chemical reaction monitored through semi-adiabatic calorimetry had given some indications towards validity of this hypothesis. XRD and FTIR studies conducted on the early age and later age solids have indicated the presence of calcium silicate hydrate further substantiating the hypothesis. These conclusions were drawn after analyzing the samples that were subjected to salicylic acid-methanol and 1:20 HCl treatment. Errors were observed in the weight measurements of insoluble residue obtained from SAM and HCl treatment. Potential reasons for errors were indentified and solutions to those problems was provided. Analysis of ion concentrations through extracted pore solution has not given much information. This is considered due to errors from sample collection which needs to be further studied.

Chapter 7

Research Output

1. "Role of slag in microstructural development and hardening of fly ash slag geopolymer" submitted to Cement and Concrete Reseach Journal and under review.

2. A poster titled, "Effects of Slag on Early Age Properties of Fly Ash-Slag Geopolymer" won the best poster award during the ACBM/AcerS conference at Purdue in July 2010.

3. A presentation titled, "Effects of Slag on Early Age Properties of Fly Ash-Slag Geopolymer" was made at ACI conference held at Tampa, Florida in April 2011.

References

[1] C.-W. Chung, "Ultrasonic wave reflection measurements on stiffening and setting of cement paste," Ph.D. dissertation, University of Illinois, Urbana Champaign, US, 2010.

[2] S. Go, C. Chung, L. Struble, and H. Lee, "Pozzolanic activity of Hwangtoh clay," *Construction and Building Materials*, vol. 24, no. 12, pp. 2638–2645, 2010.

[3] J. Davidovits, *GEOPOLYMER Chemistry and Applications*. Saint-Quentin, France: Institut Geopolymere, 2008.

[4] P. Duxson, A. Fernández-Jiménez, J. Provis, G. Lukey, A. Palomo, and J. van Deventer, "Geopolymer technology: the current state of the art," *Journal of Materials Science*, vol. 42, no. 9, pp. 2917–2933, 2007.

[5] M. Izquierdo, X. Querol, J. Davidovits, D. Antenucci, H. Nugteren, and C. Fernández-Pereira, "Coal fly ash-slag-based geopolymers: Microstructure and metal leaching," *Journal of Hazardous Materials*, vol. 166, no. 1, pp. 561–566, 2009.

[6] Jan. 2011, www.coalashfacts.org.

[7] J. Tadmore, C. Cothern, J. Smith, and D. Swaine, "Radioactive Elements in Coal and Fly Ash: Abundance, Forms, and Environmental Significance."

[8] J. Davidovits, "Geopolymers and geopolymeric materials," *Journal of Thermal Analysis and Calorimetry*, vol. 35, no. 2, pp. 429–441, 1989.

[9] Jan. 2011, http://www.epa.gov/epawaste/nonhaz/industrial/special/fossil/ccr-rule/ccr-table.htm.

[10] S. Kumar and R. Kumar, "Influence of granulated blast furnace slag on the reaction , structure and properties of fly ash based geopolymer," *Journal of Materials Science full set*, vol. 45, no. 3, pp. 607–615, 2010. [Online]. Available: http://www.springerlink.com/index/10.1007/s10853-009-3934-5

[11] J. Van Jaarsveld and J. Van Deventer, "Effect of the alkali metal activator on the properties of fly ash-based geopolymers," *Industrial & Engineering Chemistry Research*, vol. 38, no. 10, pp. 3932–3941, 1999.

[12] J. Davidovits, "Structural characterization of geopolymeric materials with x-ray diffractometry and mas nmr spectroscopy," in *Geopolymer88: First European Conference on Soft Mineralogy*, pp. 149–166.

[13] C. Yip and J. Van Deventer, "Microanalysis of calcium silicate hydrate gel formed within a geopolymeric binder," *Journal of Materials Science*, vol. 38, no. 18, pp. 3851–3860, 2003.

[14] S. Alonso and A. Palomo, "Alkaline activation of metakaolin and calcium hydroxide mixtures: influence of temperature, activator concentration and solids ratio," *Materials Letters*, vol. 47, no. 1-2, pp. 55–62, 2001.

[15] J. Davidovits, "Method for obtaining a geopolymeric binder allowing to stabilize, solidify and consolidate toxic or waste materials," July 23 1996, uS Patent 5,539,140.

[16] C. Yip, G. Lukey, J. Provis, and J. van Deventer, "Effect of calcium silicate sources on geopolymerisation," *Cement and Concrete Research*, vol. 38, no. 4, pp. 554–564, 2008.

[17] S. Antiohos and S. Tsimas, "Activation of fly ash cementitious systems in the presence of quicklime:: Part I. Compressive strength and pozzolanic reaction rate," *Cement and Concrete Research*, vol. 34, no. 5, pp. 769–779, 2004.

[18] J. Temuujin, A. Van Riessen, and R. Williams, "Influence of calcium compounds on the mechanical properties of fly ash geopolymer pastes," *Journal of Hazardous Materials*, vol. 167, no. 1-3, pp. 82–88, 2009.

[19] R. Lloyd, J. Provis, and J. van Deventer, "Microscopy and microanalysis of inorganic polymer cements. 2: the gel binder," *Journal of Materials Science*, vol. 44, no. 2, pp. 620–631, 2009.

[20] L. Struble, "The effect of water on maleic acid and salicylic acid extractions," *Cement and Concrete Research*, vol. 15, no. 4, pp. 631–636, 1985.

[21] A. Fernández-Jiménez and A. Palomo, "Mid-infrared spectroscopic studies of alkali-activated fly ash structure," *Microporous and Mesoporous Materials*, vol. 86, no. 1-3, pp. 207–214, 2005.

[22] A. Fernández-Jiménez, A. De La Torre, A. Palomo, G. López-Olmo, M. Alonso, and M. Aranda, "Quantitative determination of phases in the alkaline activation of fly ash. Part II: Degree of reaction," *Fuel*, vol. 85, no. 14-15, pp. 1960–1969, 2006.

[23] P. Hewlett, *Lea's chemistry of cement and concrete*. Butterworth-Heinemann, 2004.

[24] P. Suraneni, "Ultrasonic wave reflection measurements on self-compacting pastes and concretes," Ph.D. dissertation, University of Illinois, 2011.

[25] J. Temuujin and A. Van Riessen, "Effect of fly ash preliminary calcination on the properties of geopolymer," *Journal of Hazardous Materials*, vol. 164, no. 2-3, pp. 634–639, 2009.

[26] W. Lee and J. Van Deventer, "The effect of ionic contaminants on the early-age properties of alkali-activated fly ash-based cements," *Cement and Concrete Research*, vol. 32, no. 4, pp. 577–584, 2002.

[27] P. De SILVA and K. SAGOE-CRENSTIL, "The effect of al2o3 and sio2 on setting and hardening of na2o-al2o3-sio2-h2o geopolymer systems."

[28] M. Handke and W. Mozgawa, "Vibrational spectroscopy of the amorphous silicates," *Vibrational Spectroscopy*, vol. 5, no. 1, pp. 75–84, 1993.

[29] P. Yu, R. Kirkpatrick, B. Poe, P. McMillan, and X. Cong, "Structure of calcium silicate hydrate (c-s-h): Near-, mid-, and far-infrared spectroscopy," *Journal of the American Ceramic Society*, vol. 82, no. 3, pp. 742–748, 1999.

[30] R. R. Shagidullin, I. I. Vandyukova, A. O. Vizel, L. I. Shchukina, I. A. Studentsova, and R. S. Garaev, "Ir spectroscopy study of dimephosphon complexation with calcium chloride," *Pharmaceutical Chemistry Journal*, vol. 38, pp. 569–572, 2004, 10.1007/s11094-005-0012-4. [Online]. Available: http://dx.doi.org/10.1007/s11094-005-0012-4

[31] R. Barneyback Jr and S. Diamond, "Expression and analysis of pore fluids from hardened cement pastes and mortars," *Cement and Concrete Research*, vol. 11, no. 2, pp. 279–285, 1981.

[32] M. Cyr, P. Rivard, F. Labrecque, and A. Daidié, "High-pressure device for fluid extraction from porous materials: Application to cement-based materials," *Journal of the American Ceramic Society*, vol. 91, no. 8, pp. 2653–2658, 2008.

[33] R. Lloyd, J. Provis, and J. van Deventer, "Pore solution composition and alkali diffusion in inorganic polymer cement," *Cement and Concrete Research*, vol. 40, no. 9, pp. 1386–1392, 2010.